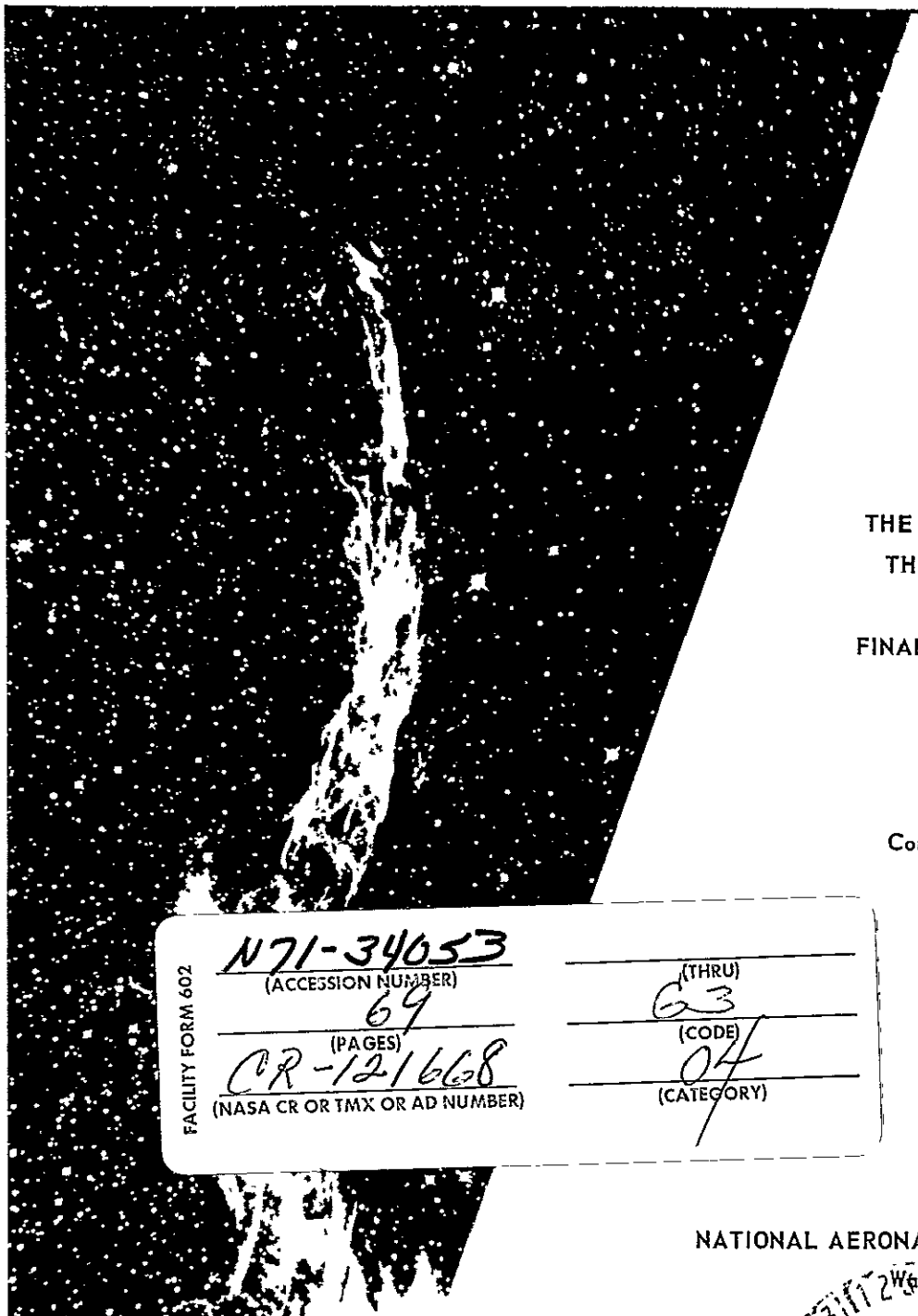

THE FLUID MECHANICS OF THROMBUS FORMATION

FINAL TECHNICAL REPORT

Contract No. NASW-1894
July 1971

prepared for

HEADQUARTERS
NATIONAL AERONAUTICS AND SPACE ADMINISTRATION
Washington, D.C. 20546

AVCO EVERETT RESEARCH LABORATORY
A DIVISION OF AVCO CORPORATION

THE FLUID MECHANICS OF THROMBUS FORMATION

FINAL TECHNICAL REPORT

prepared by

AVCO EVERETT RESEARCH LABORATORY
a division of
AVCO CORPORATION
Everett, Massachusetts

Contract No. NASW-1894

July 1971

prepared for

HEADQUARTERS
NATIONAL AERONAUTICS AND SPACE ADMINISTRATION
Washington, D.C. 20546

ABSTRACT

Experimental data are presented for the growth of thrombi (blood clots) in a stagnation point flow of fresh blood. Thrombus shape, size and structure are shown to depend on local flow conditions. The evolution of a thrombus is described in terms of a physical model that includes platelet diffusion, a platelet aggregation mechanism, and diffusion and convection of the chemical species responsible for aggregation. Diffusion-controlled and convection-controlled regimes are defined by flow parameters and thrombus location, and the characteristic growth pattern in each regime is explained. Quantitative comparisons with an approximate theoretical model are presented, and a more general model is formulated.

TABLE OF CONTENTS

		Page
	Abstract	iii
	List of Illustrations	vii
I.	INTRODUCTION	1
II.	THE EVOLUTION OF A THROMBUS ON A FOREIGN SURFACE	3
III.	THE STAGNATION POINT FLOW EXPERIMENT	11
IV.	THE STAGNATION POINT NON-NEWTONIAN BOUNDARY LAYER	15
V.	THE GROWTH OF A THROMBUS: EXPERIMENT	21
VI.	THE GROWTH OF A THROMBUS: THEORY	39
VII.	CONCLUDING DISCUSSION	57
	References	59

LIST OF ILLUSTRATIONS

Figure		Page
1	Scanning electron micrograph of an aggregated and unaggregated region.	5
2	Scanning electron micrograph of the unaggregated region of Fig. 1. Note the density of the individual spread platelets with minimal interaction between them.	6
3	Scanning electron micrograph of the aggregated region of Fig. 1. Note the density of platelets and small platelet aggregates between the larger major aggregates.	7
4	Scanning electron micrograph of thrombus in an advanced stage. Note the red cells trapped within the fibrin strands.	9
5	Schematic diagram of flow chamber in the stagnation point blood flow experiment.	12
6	Schematic diagram of a stagnation point flow field, showing non-Newtonian velocity boundary layer and platelet diffusion layer.	16
7	Thrombus "B" at 21 min. 00 sec. after start of the experiment.	22
8	Schematic diagram of thrombus growth.	23
9	Thrombus "B" at 36 min. 30 sec. after start of experiment. Note this photograph is a composite of two photographs taken during the experiment, in order to show the increase in length and width of the thrombus.	24
10	Thrombus "A" at 19 min. 00 sec.	25
11	Thrombus "A" at 38 min. 30 sec.	26
12	Growth profile of thrombus "A" as a function of time. Thrombus initiated at a radium r_i = 1.40 mm from the stagnation point. A = 16.4 sec^{-1}	27
13	Growth profile of thrombus "B", r_i = 0.75 mm, A = 16.4 sec^{-1}.	28

Figure		Page
14	Growth profile of thrombus "C", r_i = 1.55 mm, A=16.4 sec^{-1}.	29
15	Growth profile of thrombus "D", r_i=0.50 mm, A=85 sec^{-1}, at approximately 16 min. 55 sec. thrombus had completely surrounded the stagnation point.	30
16	Upstream growth of the thrombus head, Δr, from the thrombus initiation point, r_i, and the half width, w/2, of the thrombus as a function of time from the initial contanct of the blood with the surface. Thrombus "A", r_i=1.40 mm, A=16.4 sec^{-1}.	32
17	Growth of thrombus "B".	33
18	Growth of thrombus "C".	34
19	Growth of thrombus "D".	35
20	Growth of heads of four thrombi with time.	36
21	Total number of aggregate pairs vs. interaggregate distance A=10.4 sec^{-1}, r_i=0.9 mm.	37
22	Platelet aggregation sequence.	40
23	Wedge thrombus growth map.	46
24	Schematic of platelet aggregate array growth model.	51
25	Interaggregate distance as a function of time.	54

I. INTRODUCTION

The coagulation of blood is a complex phenomenon involving biochemistry, surface chemistry, and fluid mechanics. The purpose of this experimental and theoretical research is to elucidate the influence of the local flow conditions of the blood on the formation of a thrombus, particularly on artificial surfaces. To give an example of the role played by the flow, first consider the case of stagnant blood in contact with a foreign surface such as a test tube. The blood solidifies into a red clot by the formation of a stringy fibrin mesh which entraps the other constituents of the blood. In contrast to this, when flowing blood contacts a foreign surface or injured tissue, white solidified masses are observed. These masses, called thrombi, consist largely of platelets which are cells roughly one micron in size and occupy about 0.1% of the volume of whole blood. The presence of flow indeed has a marked effect on the mechanism by which blood solidifies in response to external stimuli.

It is generally accepted that high flow rates and high values of shear at the surface (short of that necessary to damage red cells) tend to minimize the incidence of thrombosis. Large shear forces on blood elements loosely attached to the surface may detach these elements before an actual thrombus is formed. A second effect is that high flow velocities imply shorter times in which the blood is in contact with the foreign surface. Some chemical reactions are required either to cause platelet aggregation or to activate the coagulation sequence. The shorter the residence time of the blood near the surface the less time is available for these reactions to proceed and, therefore, one may expect that less thrombus or no thrombus will form under conditions where the residence time is short. On the other hand, a mechanism exists by which increased flow tends to lead towards greater thrombus buildup. In the presence of high surface shears the rate at which platelets diffuse to the surface is increased. Therefore, if the surface is such that platelets stick on arrival at the surface, a high flow rate would

lead towards a more rapid accumulation of platelets and a rapid growth of the thrombus. Thus, increased flow could lead to either increased or decreased thrombosis, depending upon which of the above mechanisms is dominant. As will be described later, some evidence for each of these mechanisms has been observed.

Over the last several years a research program has been carried out[1-6] to study these fluid mechanical effects both experimentally and theoretically. A carefully controlled stagnation point flow experiment has allowed the direct observation of the above factors involved in the growth of thrombi on a foreign surface. The experimental observations suggest that diffusion of platelets to the surface, attachment of white cells within a well-defined radius of the stagnation point, and subsequent platelet aggregation in the same region are important flow dependent processes at low flow rates. However, at sufficiently high flow rates platelet aggregation and thrombus growth occur only at surface imperfections and tend to assume a characteristic wedge shape with time.

A series of observations is presented of the growth history of individual thrombi at various radial locations and flow rates. The shape, approximate thickness, and internal structure have been monitored over a sufficient range of flow conditions to demonstrate the variety of possible flow dependent growth patterns. A physical model and scaling parameters for the spatial and temporal behavior of a thrombus is also presented. A "complete" theoretical model, the final objective, remains to be developed. However, several clearly important features of the growth process have been modeled and approximate solutions obtained. Finally, quantitative comparisons with experimental data have been made where possible, and the more general analytical model outlined.

The evolution of a thrombus on an artificial surface is discussed in Section II. The experimental equipment and procedure is described in Section III. The theory of a stagnation point non-Newtonian boundary layer is reviewed in Section IV. In Section V the detailed experimental data are presented for the change of shape, size and structure of thrombi as a function of time. A general formulation of the theoretical problem is given in Section VI and the scaling laws derived from these equations are compared to the data. Section VII is the concluding discussion.

II. THE EVOLUTION OF A THROMBUS ON A FOREIGN SURFACE

When fresh blood is brought into contact with an artificial surface, a very complex chain of events is triggered which differs in numerous respects from the interaction of blood with its natural container, the blood vessel walls. In the absence of any disease which might predispose the blood to some type of hypercoagulability, the walls of the blood vessels have an antithrombogenic influence on the blood that designers of artificial devices would be pleased to emulate. When this cell wall (the endothelium) is injured, physically or chemically, a chain of events occurs which may lead to the growth of a thrombus. Although there are similarities to growth on an artificial surface, the differences, which have to do with agents released from the injured tissue, are sufficiently profound that the reader is cautioned not to directly extrapolate our description of the observed growth process to that occurring on an injured cell wall.

The first microscopically observable occurrence in the sequence is the adhesion of individual platelets to the surface[3]. This does not occur immediately, however, and the small delay time of the order of a minute is thought to be the time required for a layer of protein to be adsorbed onto the surface from the blood plasma and modified so that it becomes attractive to platelets. Although the type of surface must have some effect on the manner in which this layer is deposited, the exact nature of the interaction is unknown and a matter of controversy. A recent study by Friedman, et al[7] concludes that the platelet deposition rate is not a strong function of the type of surface, which we also noticed in earlier experiments. This could be the result of the adsorbed protein layer which physically separates the surface from the blood.

The second step is the deposition of a monolayer of platelets on the surface. The method of adhesion of the platelets to the protein layer is not known. When the process stops at this step in the sequence, which we have observed often under some flow conditions, no thrombus forms during the

duration of the experiment.

The third step is platelet aggregation. During this phase the platelets already on the surface are activated in some manner which causes them to move together along the surface into clumps. This may be accompanied by distortion of the platelet cell membrane, e. g., the platelets swell and extend outward projections called pseudopodia[8, 9]. The peculiar behavior of platelets during aggregation has been studied a great deal. See, for example, the other articles in the collections edited by Sherry, et al[10, 11] and by Johnson and Guest[12]. Other books of interest on the subject are those by Marcus and Zucker[13] and the books edited by Kowalski and Niewiarowski[14] and by Johnson, et al[15].

These platelet aggregates are illustrated in a series of scanning electron micrographs in Figs. 1 - 3. The first shows a clear dividing line between a region of heavy platelet aggregation (aggregates in white) and a region which is comparatively unaffected. The second micrograph, Fig. 2, shows individual platelets which have sent out tendril-like pseudopodia but have not yet aggregated. The larger ($\sim 8\mu$) smoother objects are red cells which were not actually attached to the surface at this point in the experiment and the presence of which is misleading. They appear only because of incomplete washing of the coverslip. In Fig. 3, the platelets are no longer individually recognizable and have aggregated into much larger clumps, the surfaces of which appear almost hairy.

Since we do not see platelet aggregates everywhere on the foreign surface, one might say that the aggregation cannot be simply a matter of reactivity between the surface and the platelets. However, we observe that surface imperfections or inhomogeneities (which may be seen optically) often are the sites of significant platelet aggregation. Complementary to this is the observation that physical bumps in the surface, but of the same general material, may significantly disturb the flow and yet not cause aggregation of platelets. One is forced to conclude that some property of the surface imperfection, whether it be a change in electronegativity or surface energy or whatever, acts as a triggering mechanism.

The biochemical processes which lead to platelet aggregation have been studied extensively. Most of these studies are performed on platelets

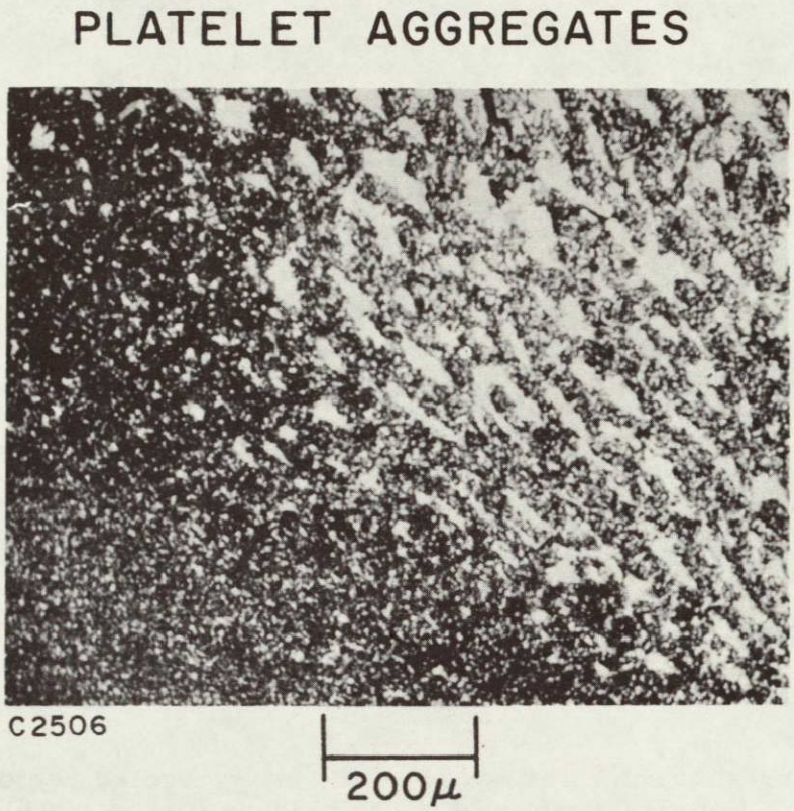

Fig. 1 Scanning electron micrograph of an aggregated and unaggregated region.

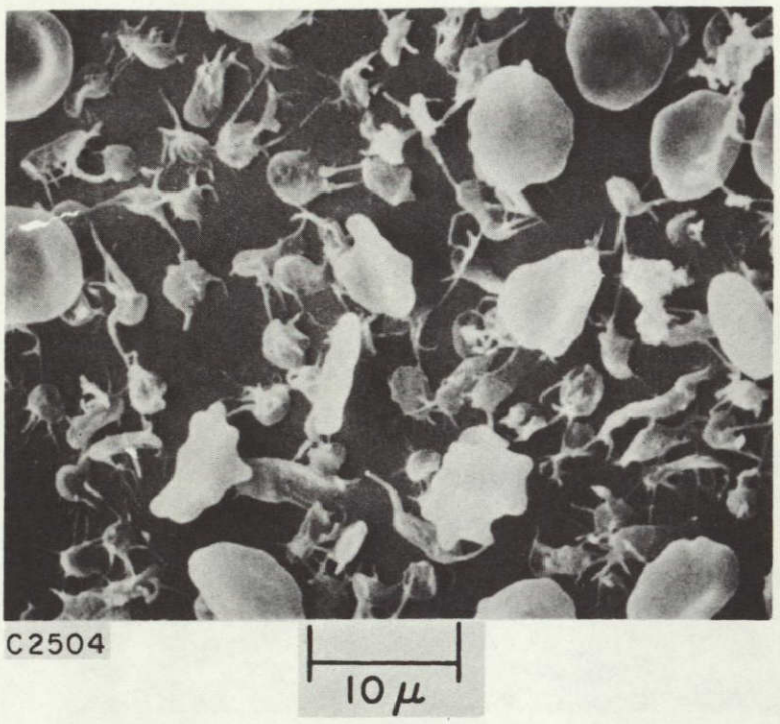

Fig. 2 Scanning electron micrograph of the unaggregated region of Fig. 1. Note the density of the individual spread platelets with minimal interaction between them.

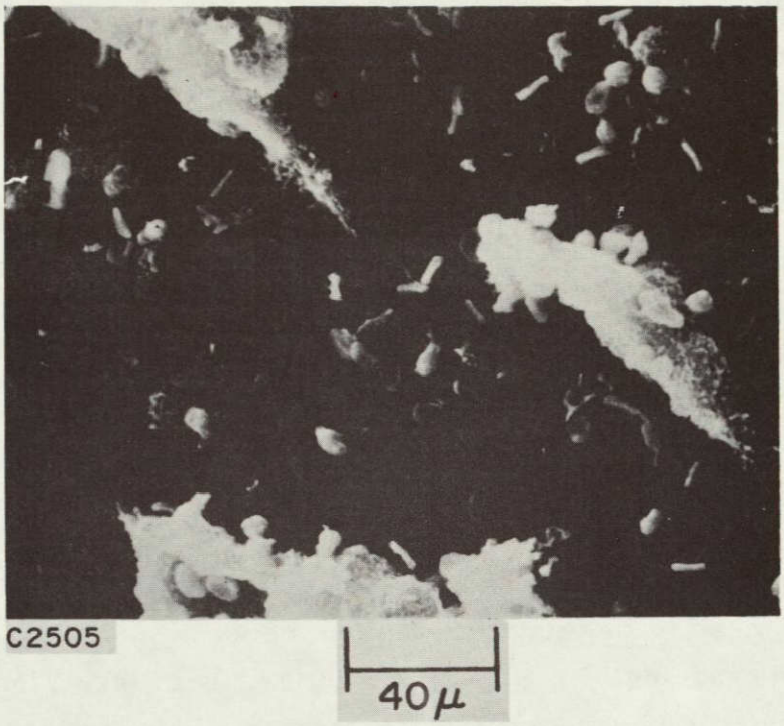

Fig. 3 Scanning electron micrograph of the aggregated region of Fig. 1. Note the density of platelets and small platelet aggregates between the larger major aggregates.

suspended in plasma. Numerous chemicals which lead to aggregation have been identified[11]. These studies do not, however, define which chemical species actually play the dominant role in platelet aggregation in flowing blood. One of the most likely candidates is ADP (adenosine diphosphate). Small concentrations of ADP lead to reversible platelet aggregation, i. e., the platelets are observed to aggregate into clumps and then deaggregate into individual platelets. Larger concentrations of ADP lead to apparently permanent aggregates. This process is believed to be accompanied by release of further ADP from the platelets themselves. The rate of accumulation of platelets on the surface is highly dependent on the local velocity profile which, as will be shown later, determines the relative diffusion rates of platelets and the species responsible for aggregation.

The processes of thrombus formation and blood coagulation (formation of a fibrin and red cell mass), while distinct, may not be entirely independent. Thrombin, which is one of the precursors in the chain of reactions which lead to fibrin formation, is also known to lead to platelet aggregation. Furthermore, the later stages of thrombus formation involve the development of a fibrin mesh in the stagnant regions between platelet aggregates, and the resultant trapping of red cells within the fibrin (see Fig. 4).

For the purpose of the present discussion, the precise nature of the chemical species which leads to platelet aggregation is not important. We shall assume that the surface imperfection which initiates the thrombus causes local platelet aggregation. Our primary concern will be with the influence of flow on the further development of the thrombus. In attempting to analyze this we will further assume that the aggregated platelets release some species which can cause further aggregation as it is convected downstream and diffuses away from the streamlines. While future work may reveal the exact chemistry of the process, it is possible to explain some of the observed features of thrombus growth based on the fluid mechanics, requiring only the above simplified assumptions concerning the complex biochemical phenomena.

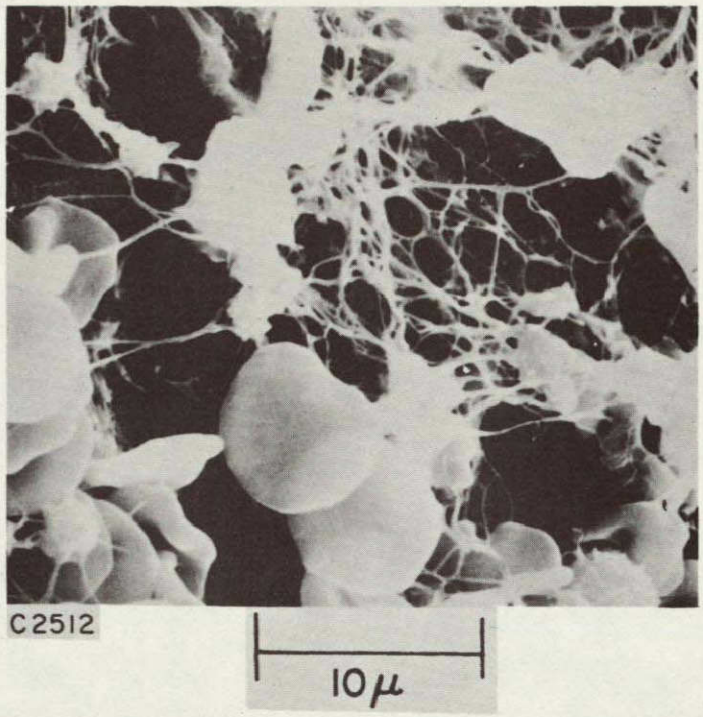

Fig. 4 Scanning electron micrograph of thrombus in an advanced stage. Note the red cells trapped within the fibrin strands.

III. THE STAGNATION POINT FLOW EXPERIMENT

In this section, the experimental procedure used for the thrombus formation study will be described. The general procedure is now routine and is utilized to study thrombus formation both as a function of hemodynamics and material surface properties.

Mongrel dogs weighing approximately 20 to 25 kg are anesthesized by intravenous injection of sodium pentobarbital. The right cartoid artery of the dog is exposed and everted over a tube which is then connected to the flow chamber. Seven flow chambers have been designed for the experiment which have inviscid flow parameters varying from 3.8 sec^{-1} to 85 sec^{-} Figure 5 is a schematic diagram of a flow chamber. The chamber is designed such that the first foreign surface which the blood contacts is the surface being studied. For this series of experiments, polyurethane surfaces were utilized. Polyurethane was selected because of its optical and relatively non-thrombogenic properties. It was solvent cast on 25 mm diameter microscope coverslips and baked in a low temperature oven with nitrogen gas flowing over the surface. This baking procedure firmly bonds the polyurethane to the glass surface, thus preventing detachment during the experiment.

The chamber is initially primed with saline to prevent the formation of an air-blood interface and the trapping of air bubbles in the chamber which result in flow pulsations. The blood is allowed to flow through the chamber at a flow rate of 2 cc/min and is collected in a withdrawal chamber. The blood is not returned to the animal, thus preventing any contamination of the blood contacting the surface by any previously "activated" blood. The flow rate through the chamber is controlled by a withdrawal system. The system is designed such that pulsations are minimized. For this series of experiments the animal was not heparinized. Heparin is added to the blood as it flows from the flow chamber into the withdrawal system. This prevents clotting in the withdrawal lines and collecting chamber.

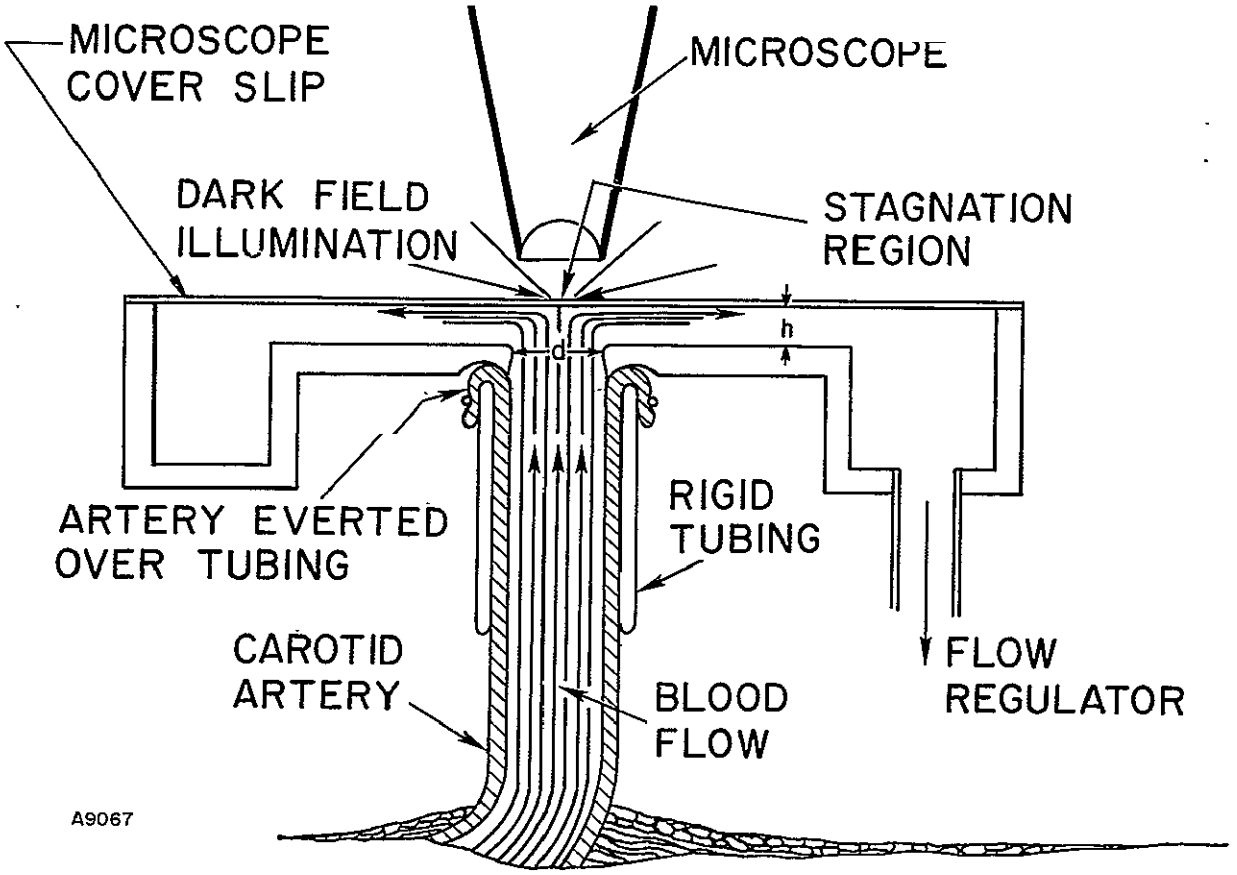

Fig. 5 Schematic diagram of flow chamber in the stagnation point blood flow experiment.

During the experiment, the blood-polyurethane surface is continually observed by dark field reflected microscopy. The location of the stagnation point and any thrombi which form are noted. When a thrombus is observed, its growth is documented by visual observations, 35 mm photographs, and 16 mm movies. Time at which flow distortion begins to occur, reverse or lateral flow, and red cell trapping are observed visually. Approximate aggregate depth is obtained by utilizing a 22 X objective lens and a micrometer scale on the focus adjustment of the microscope. The lens is first focused on the blood-polyurethane surface, and then focused through the aggregates on the blood cells flowing over the aggregates.

Local white cell velocity data and thrombi growth profiles are obtained from the 16 mm movies. Profiles and interaggregate distance are also obtained from 35 mm slides.

At the conclusion of the experiment, the dog is sacrificed and the coverslips are stained with Wrights stain and examined.

IV. THE STAGNATION POINT NON-NEWTONIAN BOUNDARY LAYER

The flow of blood on the surface of the coverslip is modeled as axisymmetric stagnation point flow of a continuous viscous fluid having a non-Newtonian stress-strain relationship. In the absence of viscous effects, the velocity components would be given by the potential flow solution

$$u = +Ar, \quad v = -2Az \tag{1}$$

where r, z are the radial and normal coordinates and u, v the corresponding velocity components. The flow field is illustrated schematically in Fig. 6. The constant A is the stagnation point flow parameter, which represents the radial velocity gradient of the fluid at the edge of the boundary layer as it accelerates away from the stagnation point. The above velocity field is only valid for distances from the surface large compared to the boundary layer thickness. For a Newtonian fluid this thickness is given by[16]

$$\delta_N = 2.4\,(\nu/A)^{1/2} \tag{2}$$

where $\nu \simeq .04$ cm^2/sec is the kinematic viscosity of blood at high rates of shear where blood is Newtonian. To get some appreciation of relative sizes we can calculate that for A = 10 sec^{-1} this thickness is $\delta_N = 0.15$ cm which is about the characteristic size of our flow chambers and is about 190 red cell diameters.

It is in fact the presence of the red cells which causes blood to have a non-Newtonian behavior at low shear rates, for the disk-like red cells have a propensity to form long chains (rouleaux) not unlike stacks of poker chips. The adhesion of the red cells to one another, which is thought to be caused by the adsorption of fibrinogen on the surface of the cells, may be broken at higher shear rates and therefore blood is what is termed in rheology a pseudoplastic, or shear-thinning fluid. A non-Newtonian stress-strain law which adequately fits the experimental data[17] is the power law

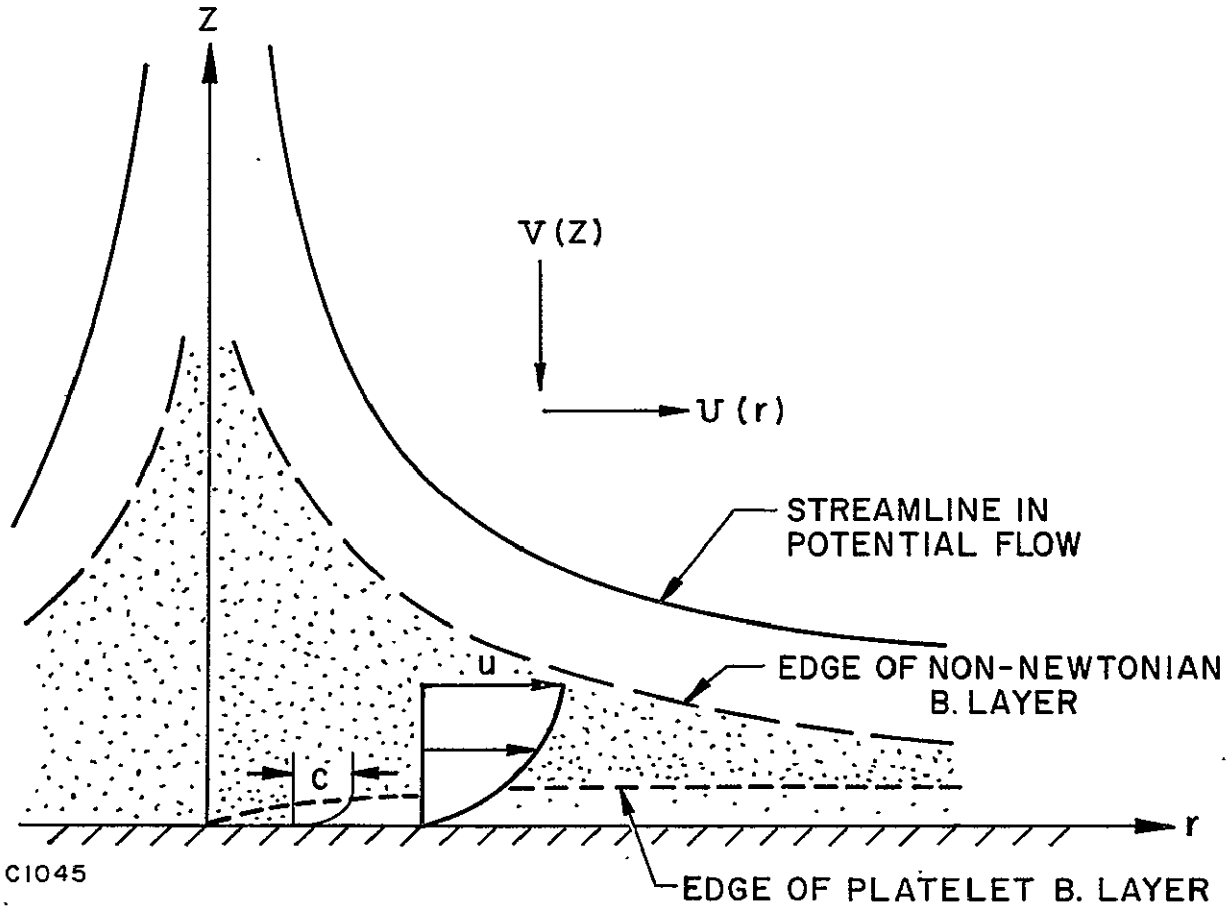

Fig. 6 Schematic diagram of a stagnation point flow field, showing non-Newtonian velocity boundary layer and platelet diffusion layer.

$$\tau = K(\partial u/\partial z)^N \tag{3}$$

where τ is the shear stress, $\partial u/\partial z$ the rate of strain and K, N are constants. Blood of normal hemocrit (45% red cells by volume) may be represented[18,19] by the values $N = 4/5$, $K = 0.1$ in cgs units. Correspondingly, one may consider blood to have a rate of strain dependent viscosity of $\mu \approx 0.1\,(\partial u/\partial z)^{-0.2}$ gm cm^{-1} sec^{-1}. The above approximations should be adequate for the boundary layer analysis which follows.

The axisymmetric stagnation point boundary layer equations are

$$\rho u\, \partial u/\partial r + \rho v\, \partial u/\partial z = \partial \tau/\partial z - \partial p/\partial r \tag{4}$$

$$\partial u/\partial r + u/r + \partial v/\partial z = 0 \tag{5}$$

for the conservation of radial momentum and conservation of mass. The shear stress is given by Eq. (3) and the pressure gradient is $\partial p/\partial r = -\rho A^2 r$ from the irrotational flow represented by Eq. (1). It is convenient to nondimensionalize all the lengths and velocities by the reference length $\ell = (\nu_R/A)^{1/2}$ and the velocity $U = (\nu_R A)^{1/2}$ where ν_R is a reference viscous diffusivity to be chosen momentarily and A is the stagnation point flow parameter. Letting

$$(\bar{u},\ \bar{v}) = (u/U,\ V/U);\ (\bar{r},\ \bar{z}) = (r/\ell,\ z/\ell) \tag{6}$$

we have for the dimensionless conservation equations

$$\bar{u}\frac{\partial \bar{u}}{\partial \bar{r}} + \bar{v}\frac{\partial \bar{u}}{\partial \bar{z}} = \left(\frac{\partial \bar{u}}{\partial \bar{z}}\right)^{N-1}\frac{\partial^2 \bar{u}}{\partial \bar{z}^2} + \bar{r} \tag{7}$$

$$\frac{\partial \bar{u}}{\partial \bar{r}} + \frac{\bar{u}}{\bar{r}} + \frac{\partial \bar{v}}{\partial \bar{z}} = 0 \tag{8}$$

if the reference kinematic viscosity is chosen as

$$\nu_R = \frac{NK\,A^{N-1}}{\rho} \tag{9}$$

The proper nondimensionalizing length and velocity are then

$$\ell = \left(\frac{NK\,A^{N-2}}{\rho}\right)^{1/2}, \quad U = \left(\frac{NK\,A^{N}}{\rho}\right)^{1/2} \tag{10}$$

The above system of partial differential equations, (7) and (8), may be reduced to one ordinary differential equation in one independent variable using the similarity transformation implied by the following equations

$$\eta = \bar{z}\,\bar{r}^{\frac{1-N}{1+N}} \tag{11}$$

$$\bar{u} = \bar{r}\,\phi'(\eta) \tag{12}$$

$$\bar{v} = -\bar{z}\left[\left(\frac{3N+1}{N+1}\right)\frac{\phi}{\eta} + \left(\frac{1-N}{1+N}\right)\phi'\right] \tag{13}$$

The differential equation is

$$(\phi')^{N-1}\phi''' + \frac{3N+1}{N+1}\phi\phi'' - (\phi')^2 + 1 = 0 \tag{14}$$

with the boundary conditions

$$\phi(0) = \phi'(0) = 0, \quad \phi'(\infty) = 1 \tag{15}$$

The numerical solutions to (14) may be found in Ref. 20 where $\phi'(\eta)$ and $\phi''(0)$ are tabulated for various values of N.

The velocity gradient and the shear stress at the surface are given in physical coordinats for a non-Newtonian fluid by

$$\left(\frac{\partial u}{\partial z}\right)_w = \left(\frac{\rho A^3 r^2}{NK}\right)^{\frac{1}{N+1}} \phi''(0) \tag{16}$$

$$\tau_w = K\left(\frac{\rho A^3 r^2}{NK}\right)^{\frac{1}{N+1}} (\phi''(0))^N \tag{17}$$

The relevant constants that have not yet been given are $\phi''(0) \approx 1.25$ for any N near unity and $\rho \approx 1.06$ gm/cm^3.

For a Newtonian fluid, the shear at the surface can be shown to increase as the 3/2 power of the flow parameter, A, and to increase linearly with distance from the stagnation point. Thus, for a given flow parameter, the shear is zero at the stagnation point and increases as one moves outward. The shear at any given distance from the stagnation point is larger the higher the flow parameter. The radius at which a given shear is reached decreases as the 3/2 power of the flow parameter. Thus, for a situation in which local shear is the significant parameter, one would expect similar phenomena to occur at radii which decrease with increasing flow as the 3/2 power of the flow parameter. For some of the results to be described later, the departure of blood from a Newtonian viscosity is significant. In this case the shear still increases with radial distance from the stagnation point. However, its variation with distance is different. It can be shown, however, based on an analysis of non-Newtonian stagnation flow, that the radius at which a given shear is reached still scales as the inverse 3/2 power of the flow parameter.

For comparison to experiment it is useful to approximate the velocity profile in this thin viscous layer as a linear variation with the distance z away from the surface. In the viscous layer then

$$u = \beta \; rz \tag{18}$$

where we have defined a convenient parameter $\beta = (\partial u/\partial z)_w r^{-1}$.

The parameter β is theoretically well defined only for the ideal stagnation point flow, the streamlines of which are hyperbolic in shape as shown in Fig. 6. Since the flow in the experimental flow chambers does not correspond exactly to this ideal, the parameter β has been measured empirically. This also allows the determination of an effective inviscid stagnation point flow parameter, A, for a given flow rate of blood through a given chamber.

This discussion of the velocity field in the flow experiment forms a framework for the following presentation of the data taken on the growth of thrombi.

V. THE GROWTH OF A THROMBUS: EXPERIMENT

Numerous experiments have been carried out according to the procedure outlined in Section III. The data to be presented here have been selected as typical of the numerous thrombi we have observed. Other data were rejected for various reasons, e.g., some thrombi could not be observed over a long enough time interval or over a large enough area; others occurred so close together in one run that their growth was dominated by mutual interference effects. The four thrombi (Labeled A, B, C, D) which we show here are the best documented examples.

The photographs of the four thrombi are black and white reproductions of single frames of the color movies taken through the optical microscope. The first photograph, Fig. 7, shows thrombus B at a very early stage. What can be seen as a faint airfoil shape is the region of platelet aggregation and white cells in the wake of the point of initiation. A schematic picture of the growth of the region of platelet aggregation with time is furnished in Fig. 8. A picture of the same thrombus at a later intermediate time is given in Fig. 9. Note the swept back wedge-like shape of the thrombus and the mottled appearance and nonuniform nature of the platelet aggregation. The picture of thrombus A in Fig. 10 clearly shows the characteristic shape of the head or leading edge of the wedge thrombus, and the initiation point (a surface imperfection) shows up as a bright spot. The last photo of thrombus A in Fig. 11 shows the shape at a later time when the growth has been greatly influenced by the radial nature of the flow. The radius of curvature of the indentation of the head of the thrombus is nearly equal to the radius from the stagnation point. Some thrombi, such as thrombus D, eventually grow to envelop the stagnation point, and thereafter rapidly cover the entire surface.

Quantitative data chronicling the growth history of the thrombi are presented in three ways. First, in Figs. 12-15 the outlines of the greatest extent of the platelet aggregation as perceived visually are given as a

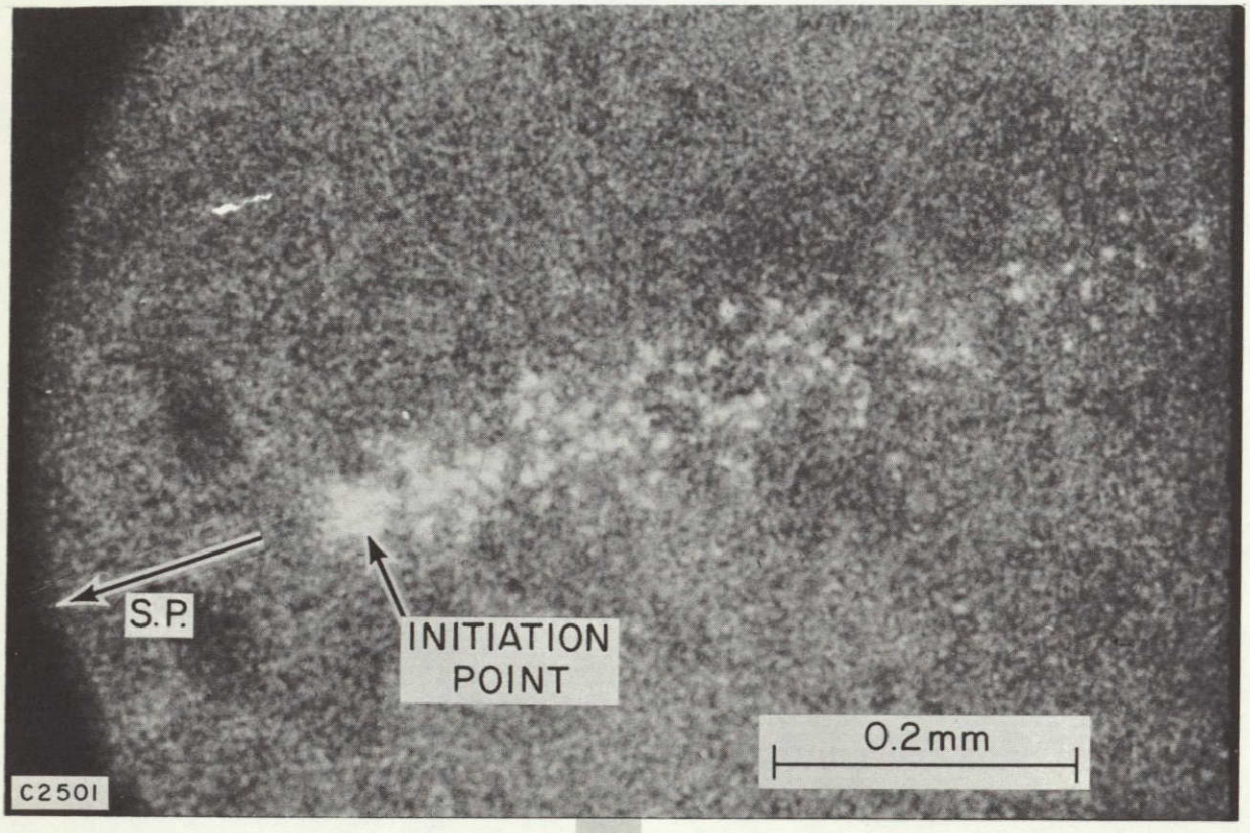

Fig. 7 Thrombus "B" at 21 min. 00 sec. after start of the experiment.

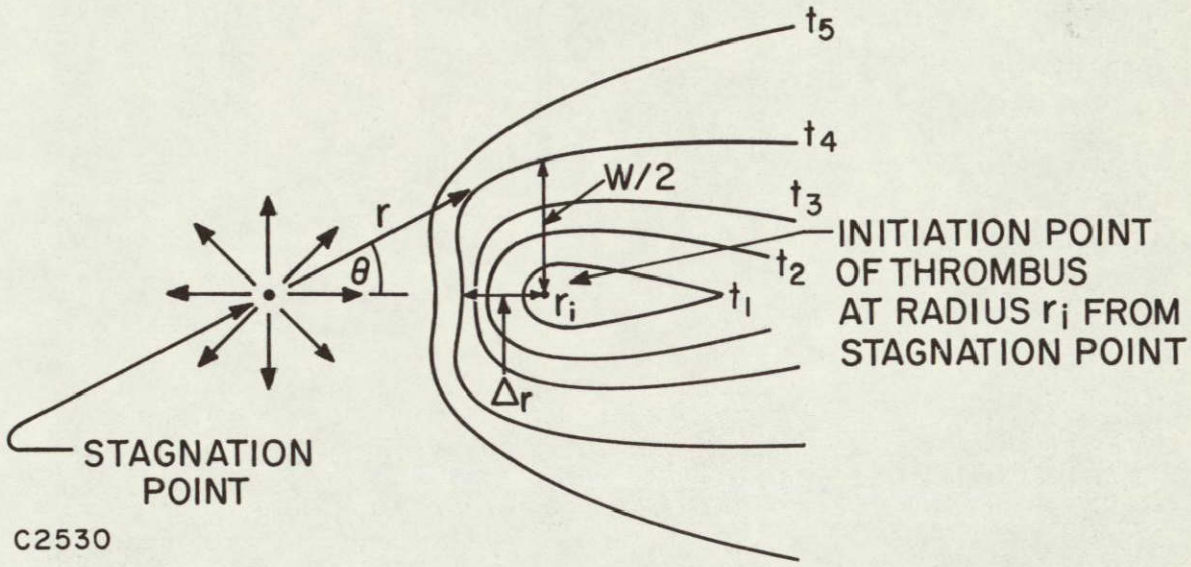

Fig. 8 Schematic diagram of thrombus growth.

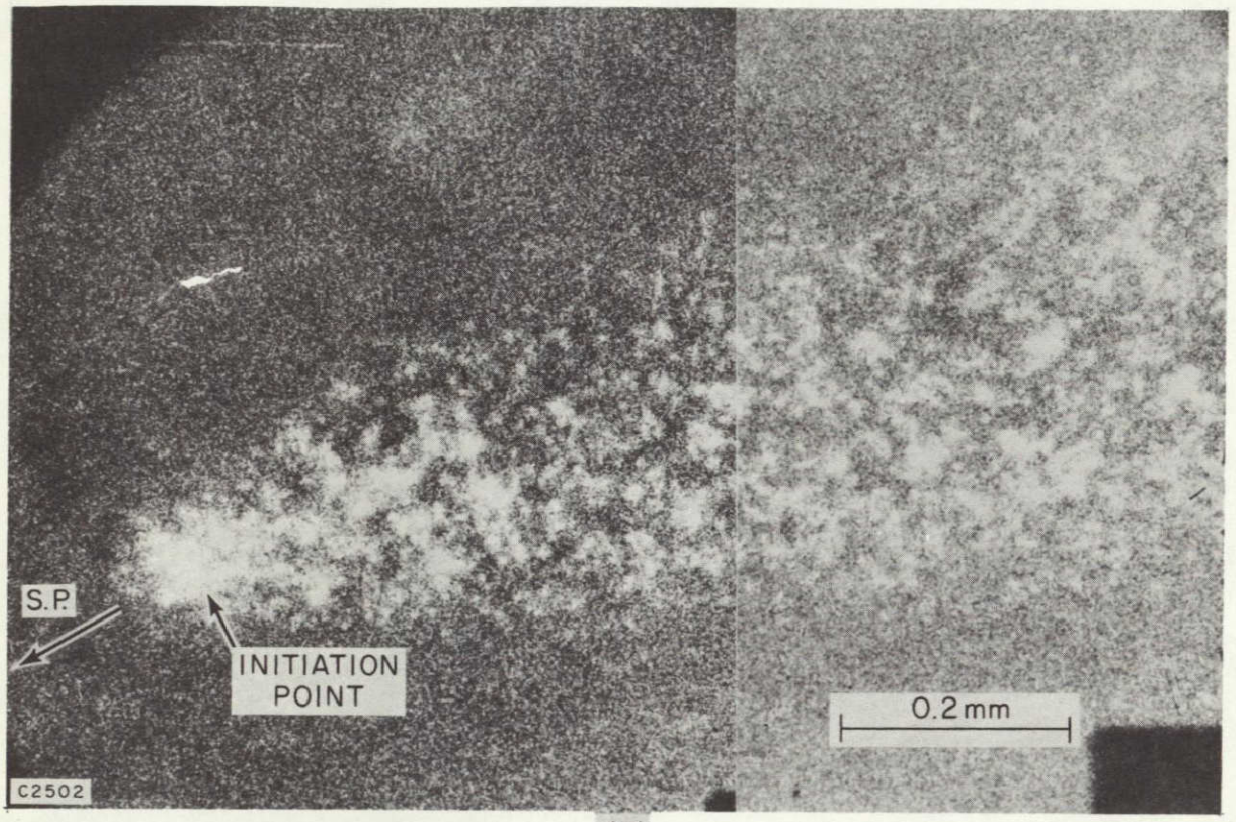

(B)

Fig. 9 Thrombus "B" at **36 min.** 30 sec. after start of experiment. Note this photograph is a composite of two photographs taken during the experiment, in order to show the increase in length and width of the thrombus.

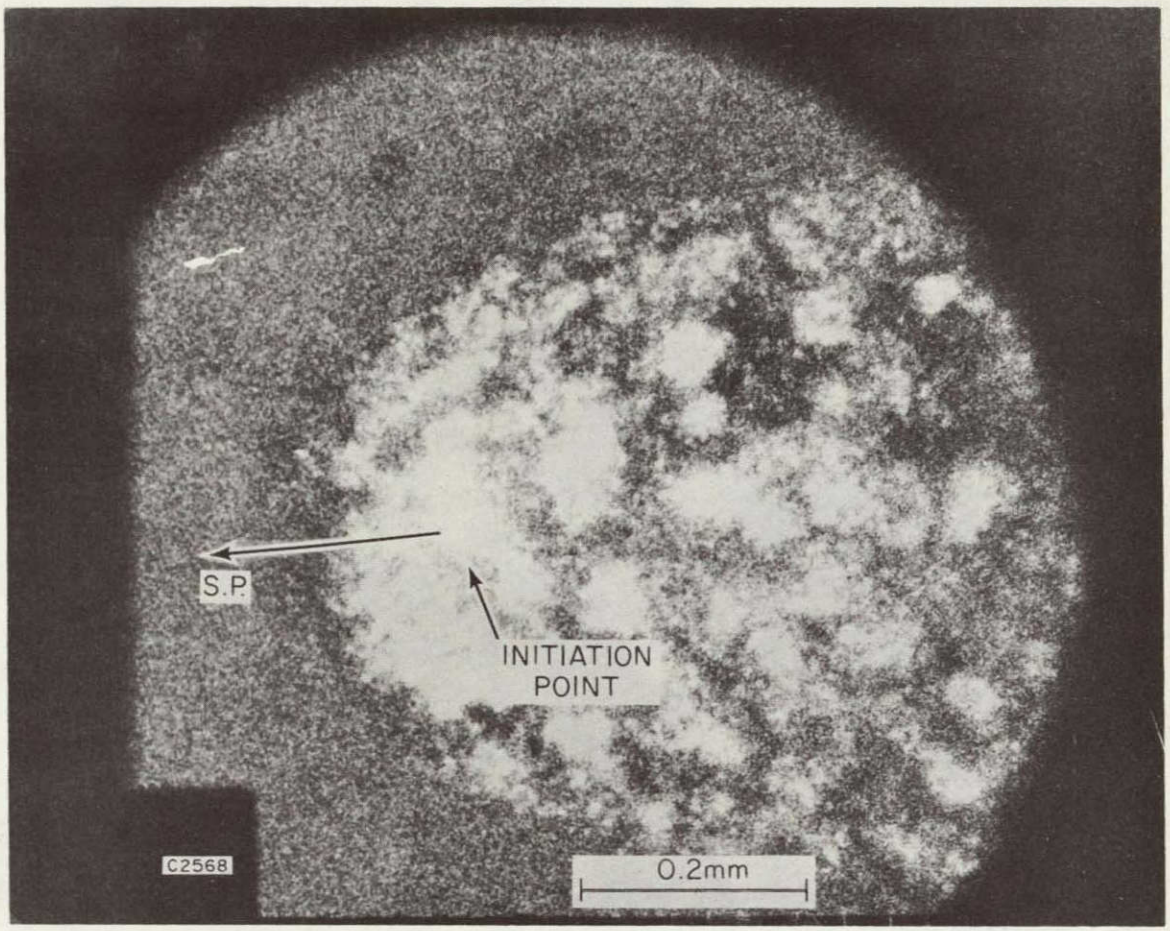

Fig. 10 Thrombus "A" at 19 min. 00 sec.

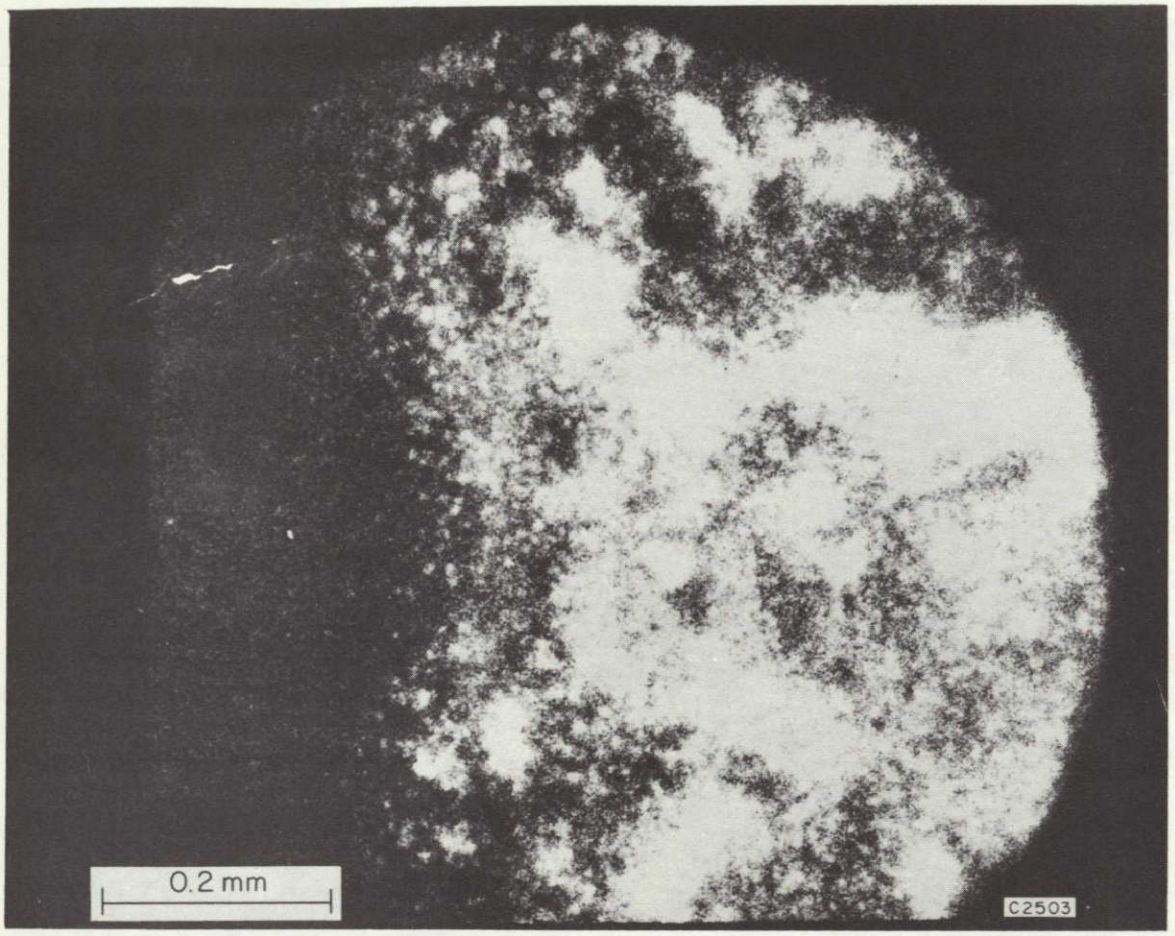

Fig. 11 Thrombus "A" at 38 min. 30 sec.

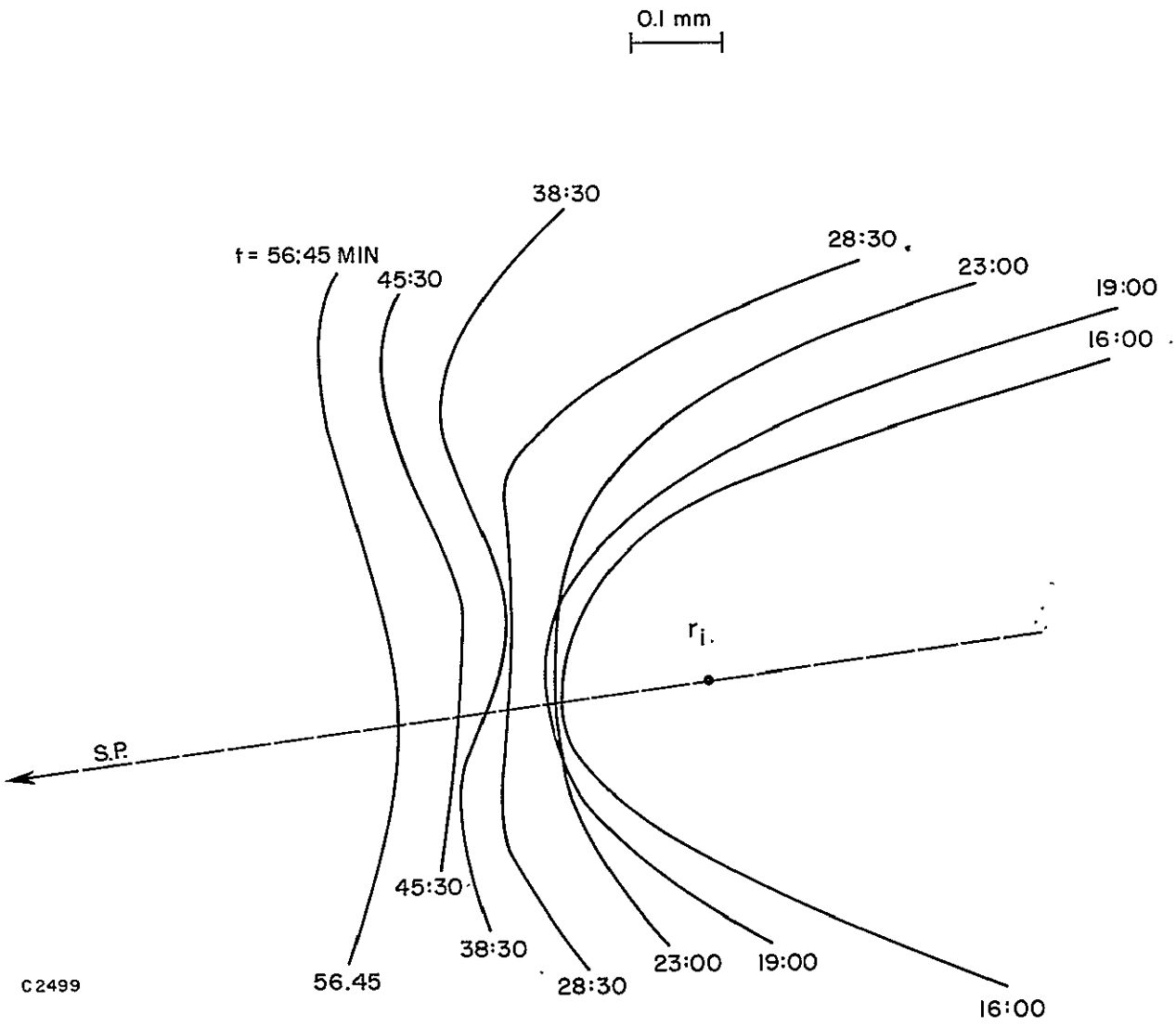

Fig. 12 Growth profile of thrombus "A" as a function of time. Thrombus initiated at a radium r_i = 1.40 mm from the stagnation point. A = 16.4 sec^{-1}.

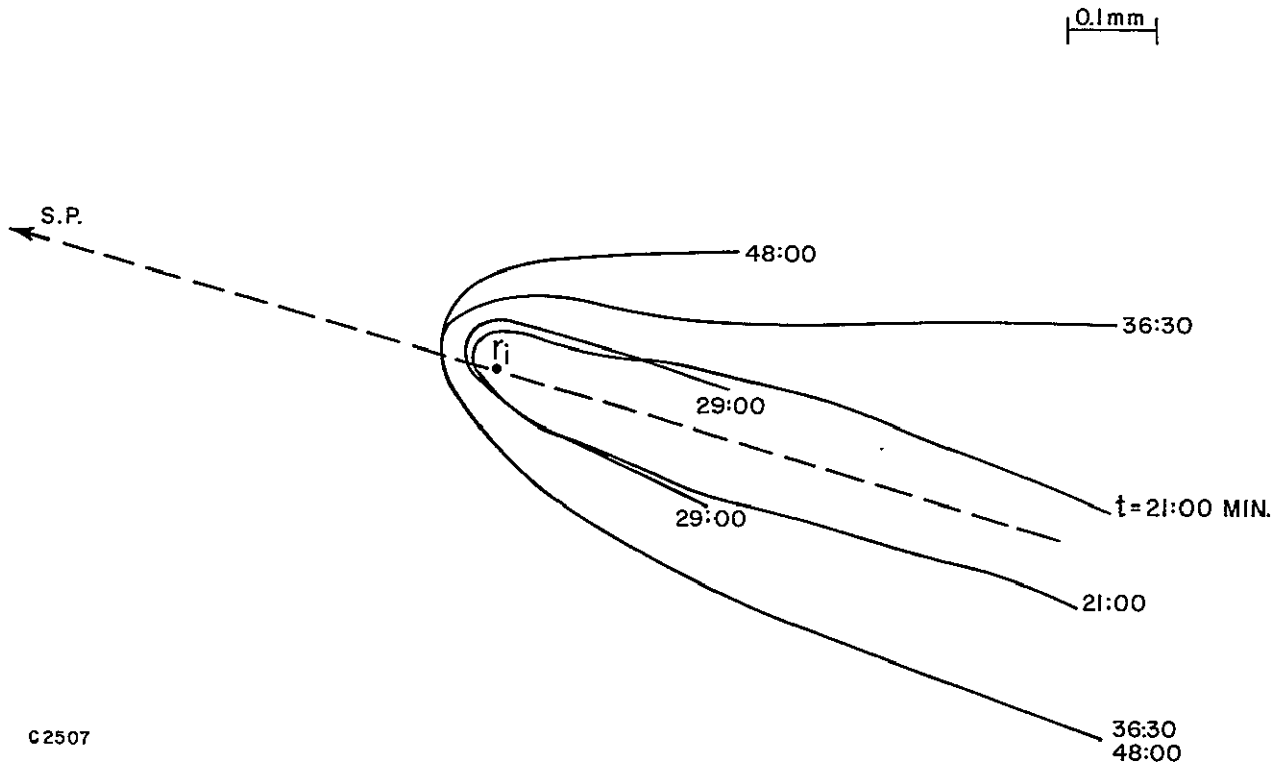

Fig. 13 Growth profile of thrombus "B", r_i = 0.75 mm, A = 16.4 sec^{-1}

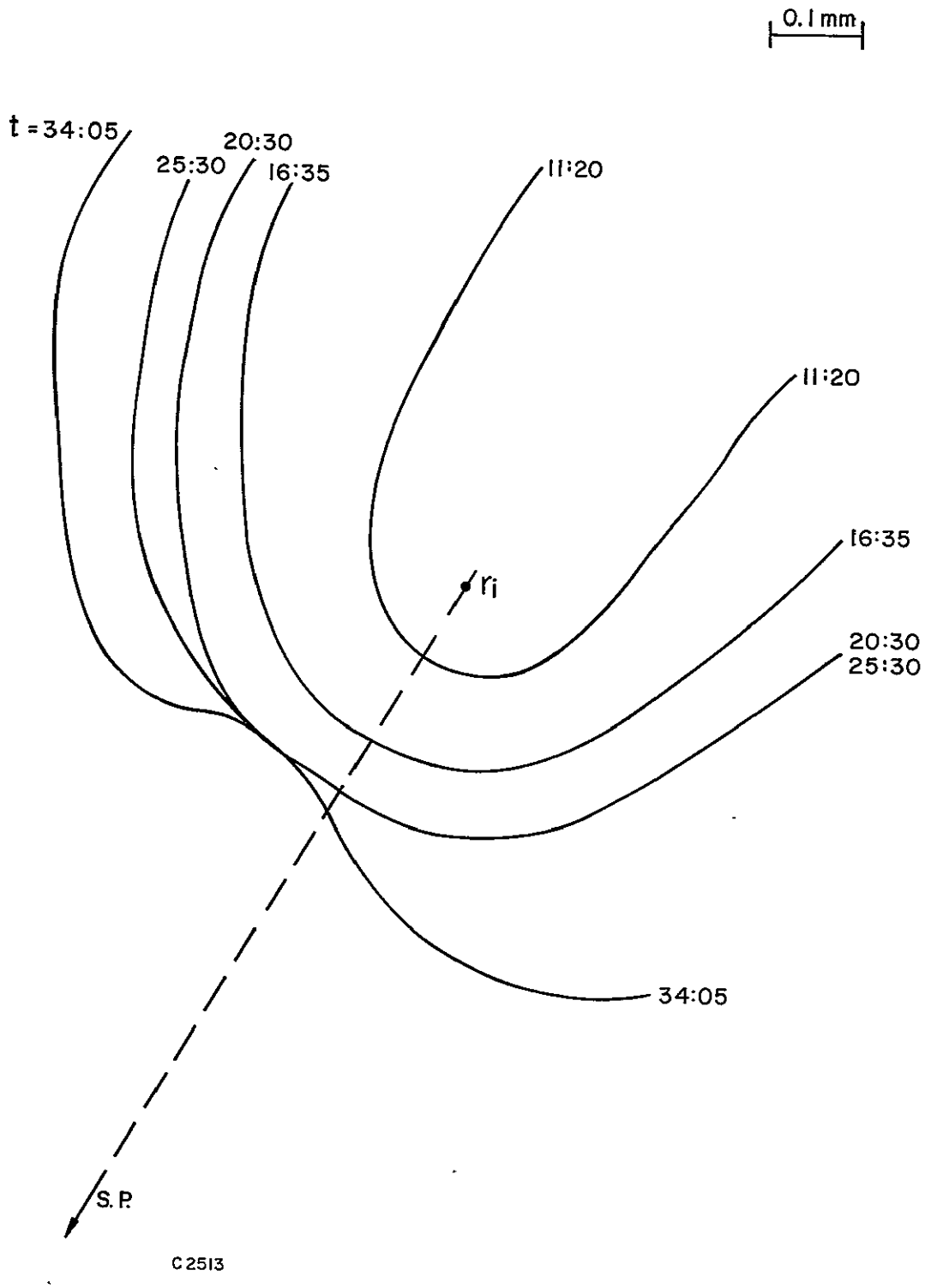

Fig. 14 Growth profile of thrombus "C", r_i = 1.55 mm, A = 16.4 sec^{-1}.

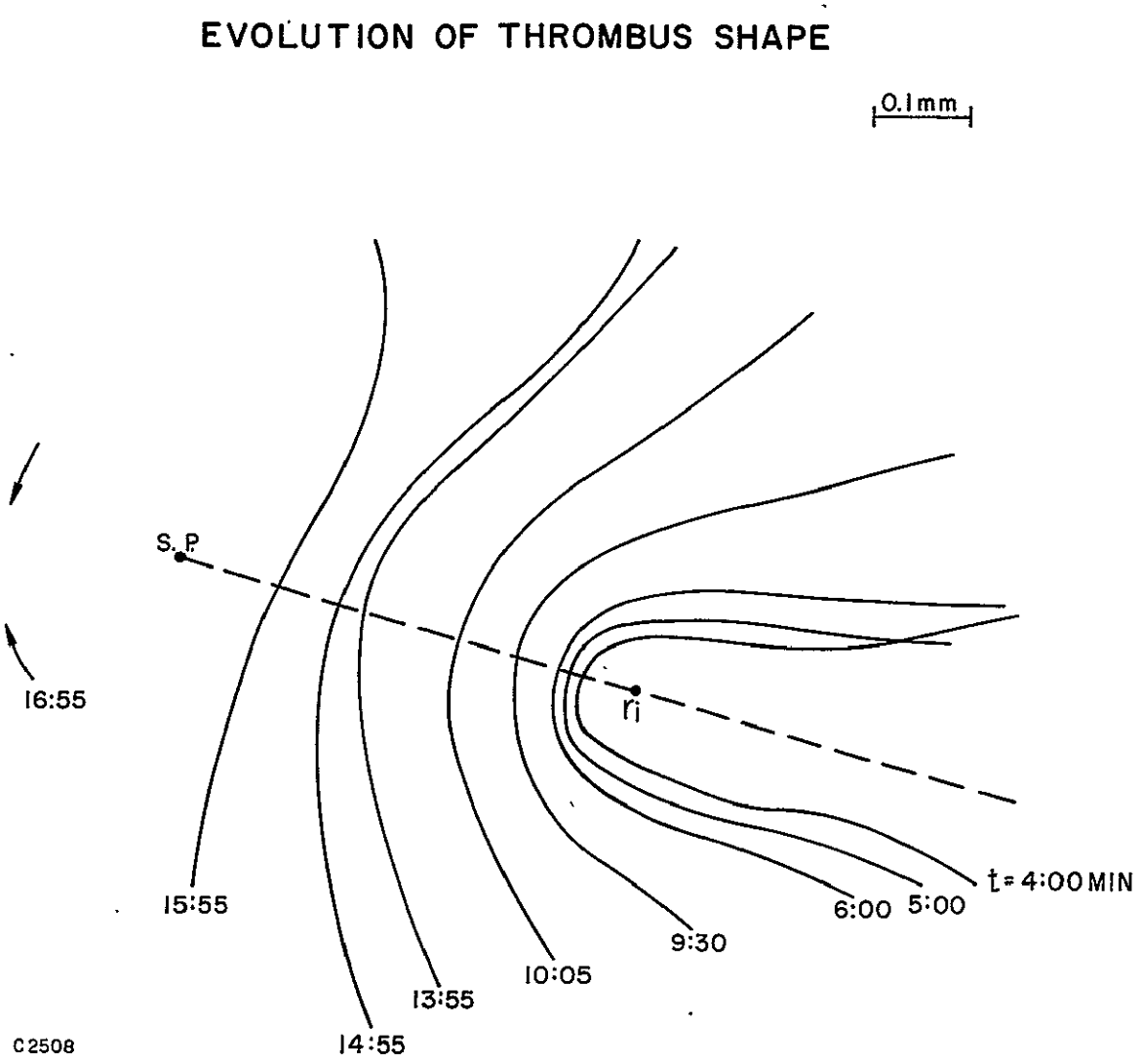

Fig. 15 Growth profile of thrombus "D", r_i = 0.50 mm, A = 85 sec^{-1}, at approximately 16 min. 55 sec. thrombus had completely surrounded the stagnation point.

function of time for each of the four thrombi. Secondly, data on the growth of the head toward the stagnation point and on the width of the head is presented in Figs. 16-19. These measurements are illustrated in the schematic of Fig. 8. In Fig. 20 we have graphed the thrombus head position as a function of time for the four thrombi grown under different flow conditions. The third set of data is given in Fig. 21 and represents statistics on the inter-aggregate spacing in a thrombus as a function of distance from the stagnation point and time. The data is presented in the form of histograms of measured interaggregate distances at three times during the experiment. A "best fit" curve is drawn through the total set of measurements at each time.

It is clear that a theoretical description of these effects must consider the transport to the surface of molecular and cellular matter suspended in the blood as well as the surface reactions. The characteristic size, shape and structure of the wedge thrombi discussed above are qualitatively well understood in terms of the model which is formulated in the following section.

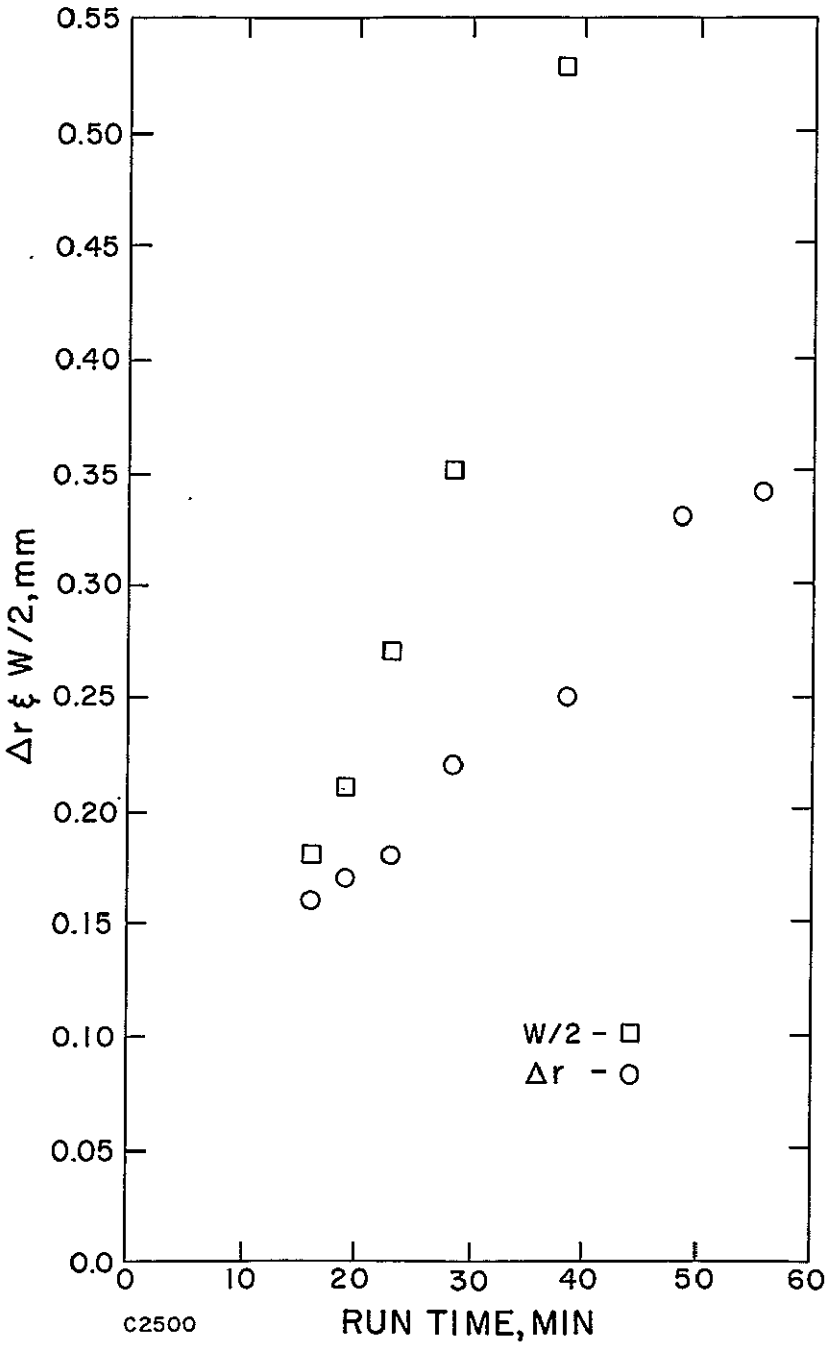

Fig. 16 Upstream growth of the thrombus head, Δr, from the thrombus initiation point, r_i, and the half width, $w/2$, of the thrombus as a function of time from the initial contact of the blood with the surface. Thrombus "A"; r_i = 1.40 mm, A = 16.4 sec^{-1}.

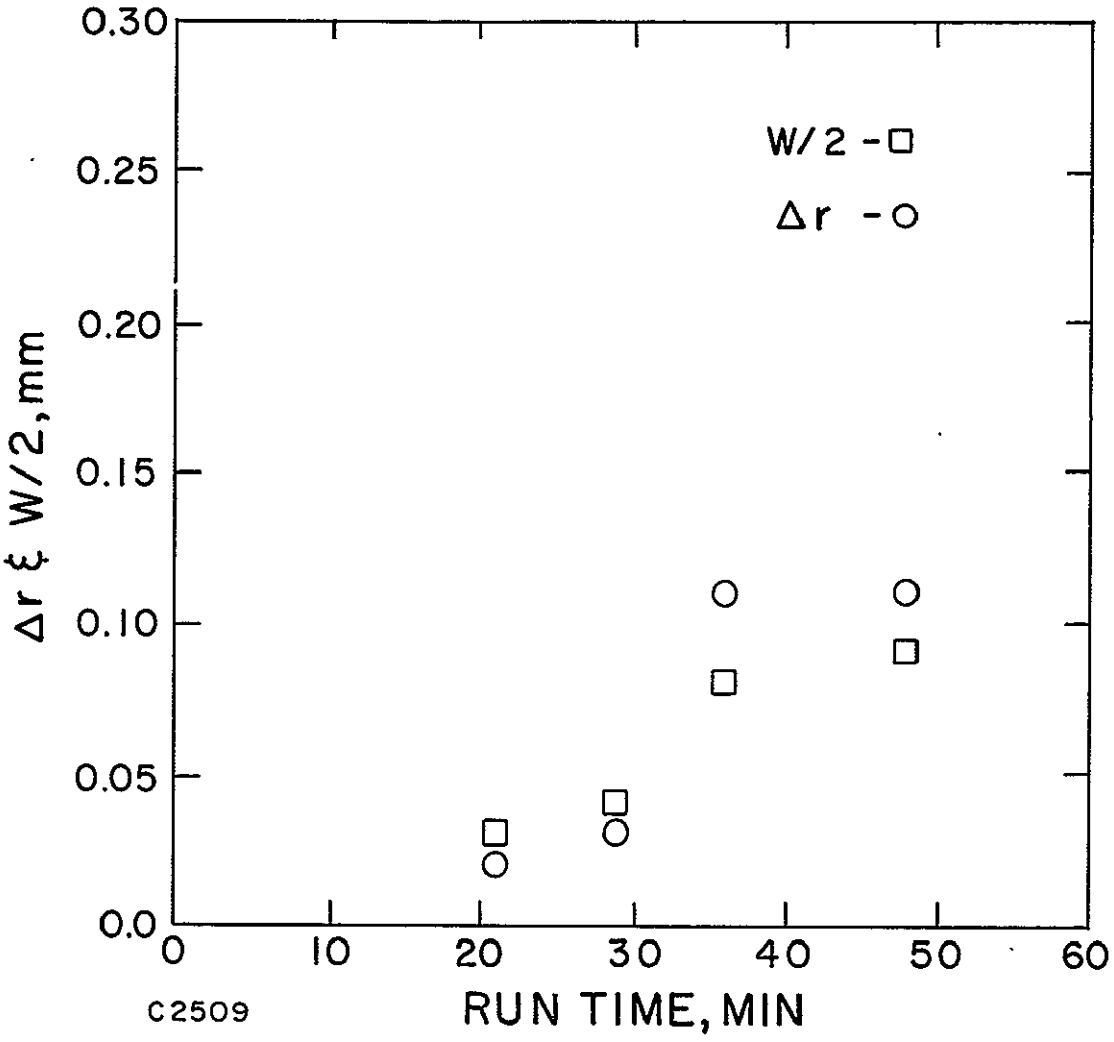

Fig. 17 Growth of thrombus "B".

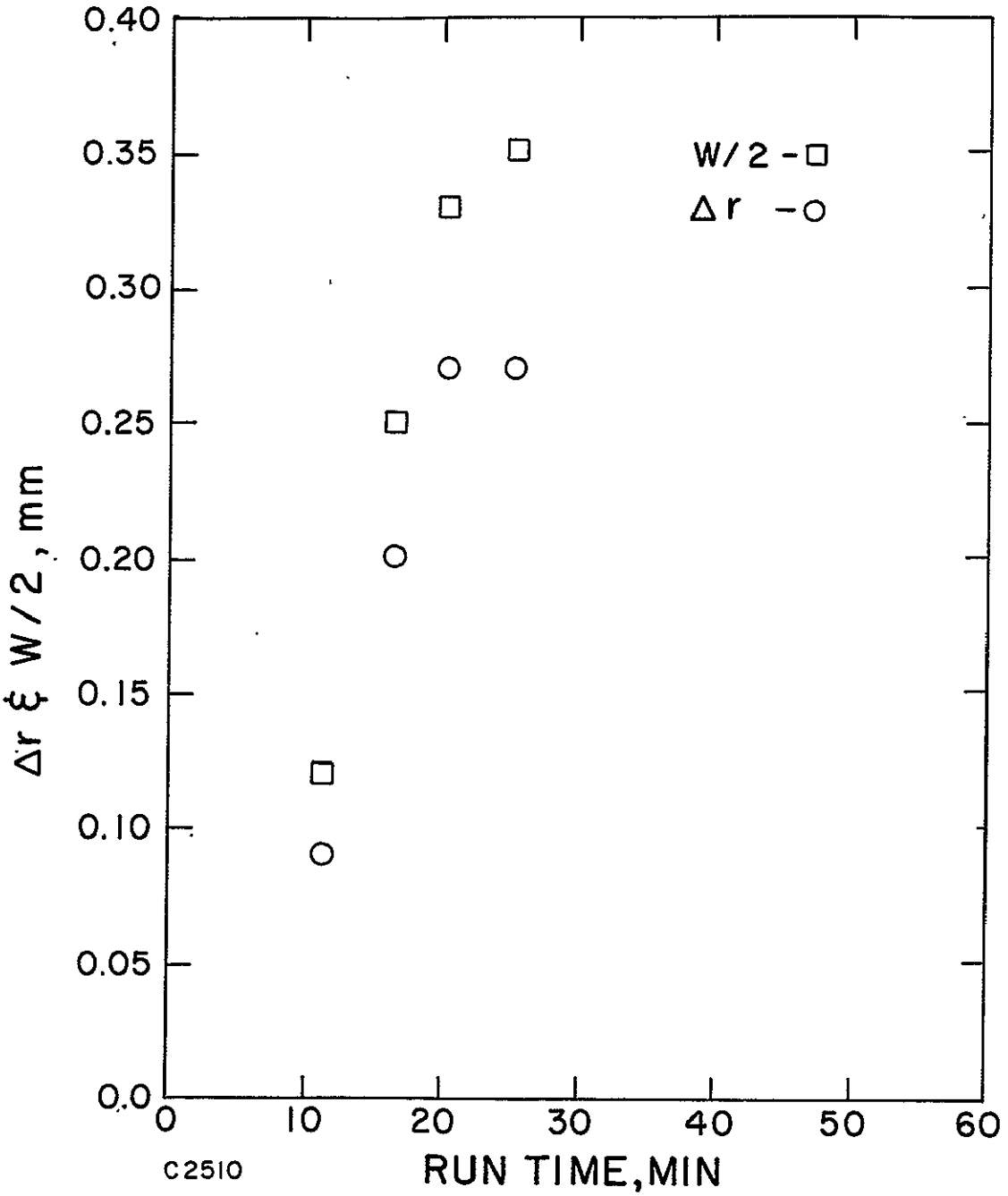

Fig. 18 Growth of thrombus "C".

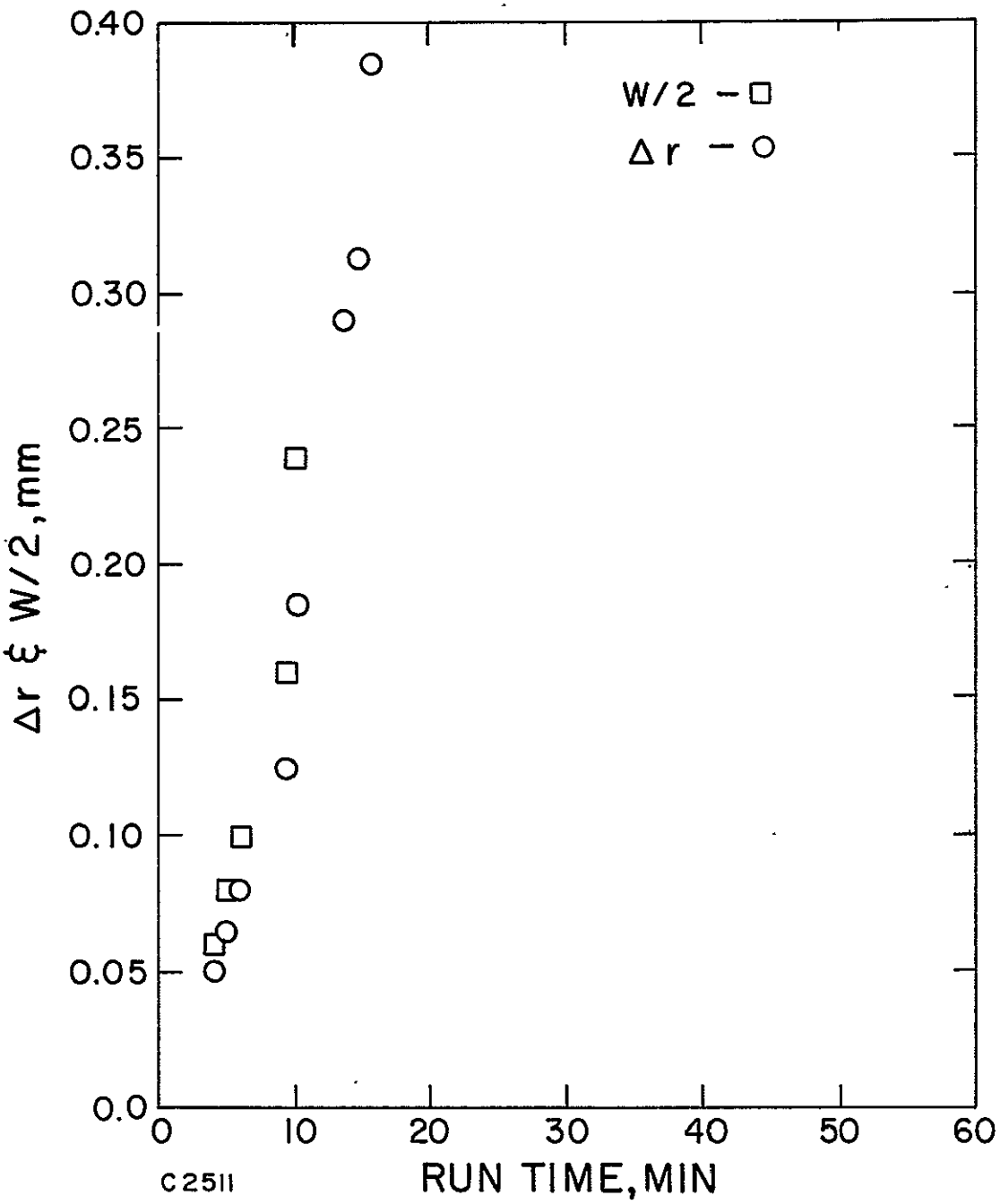

Fig. 19 Growth of thrombus "D".

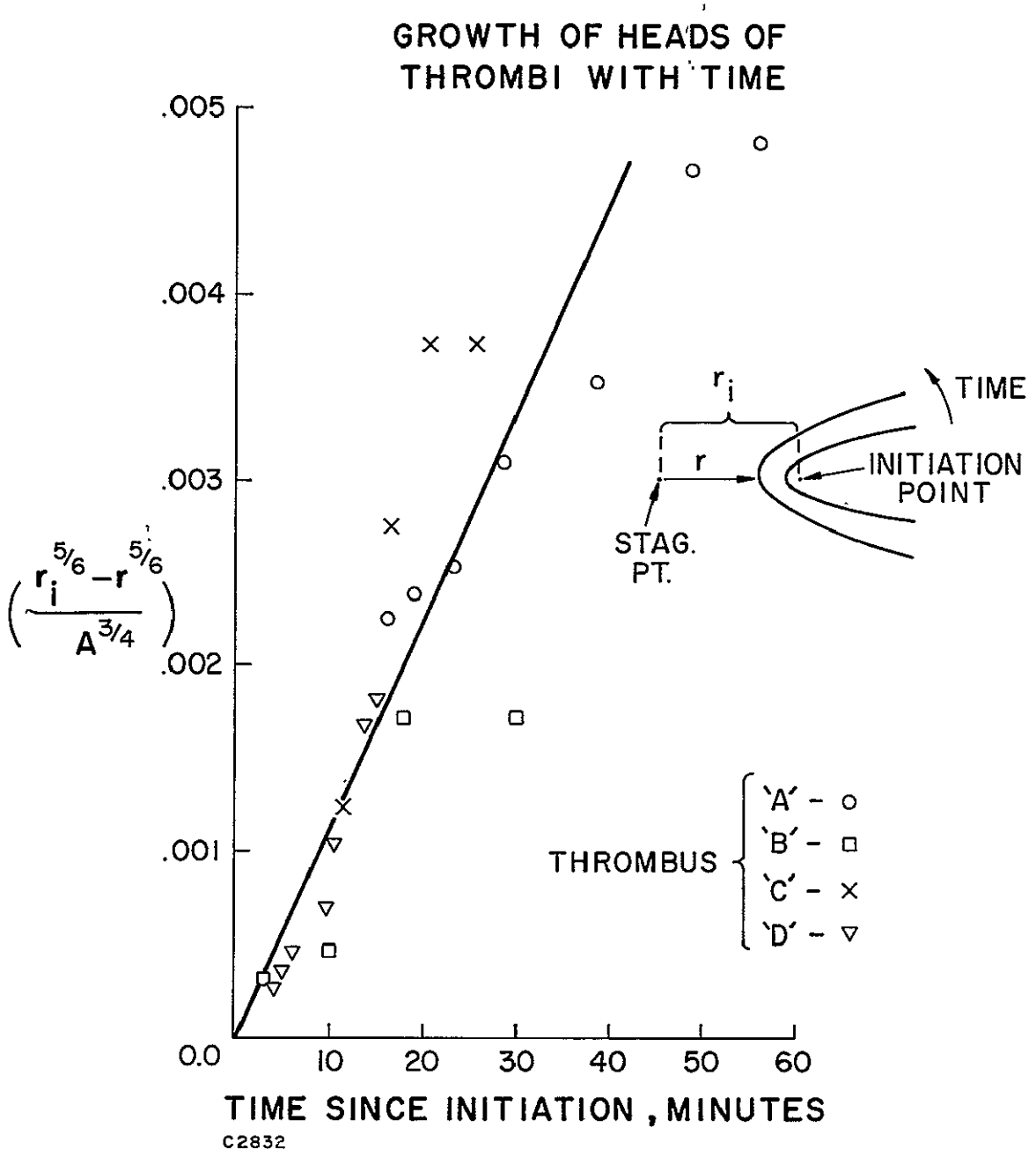

Fig. 20 Growth of heads of four thrombi with time.

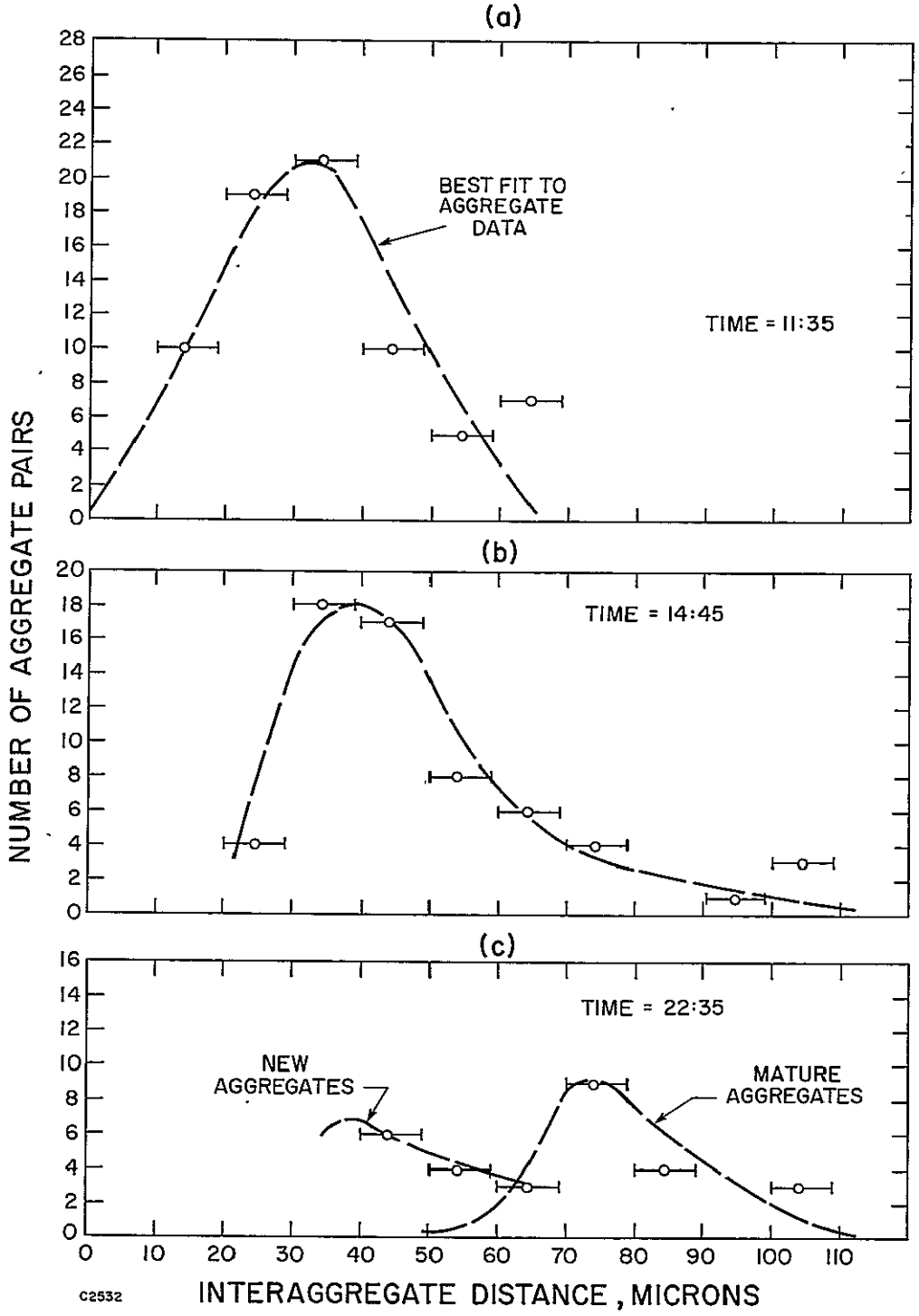

Fig. 21 Total number of aggregate pairs vs. interaggregate distance $A = 10.4\ sec^{-1}$, $r_i = 0.9$ mm.

VI. THE GROWTH OF A THROMBUS: THEORY

Part I - Early and Intermediate Time

In the section describing the evolution of a thrombus, a two-part mechanism of platelet aggregation and accumulation is postulated which utilizes the concept of an activating species which is contained in the platelets themselves. When a platelet encounters a critical concentration of this species near the surface, it sticks to the surface and joins in the aggregation, in which process more of the species is released to activate other platelets. This process is graphically described in the flow chart of Fig. 22. The growth of the aggregate can be limited only by a shortage in the release rate of the activating species or a shortage in the arrival rate of platelets. Now, we would like to quantify these concepts in the construction of a mathematical model capable of describing the features of thrombus growth which have been documented in Sec. V.

The platelets are the dominant constituent in the thrombi we observe. We shall derive a conservation equation for them presently. Before doing this, however, we must give attention to the dominant transportation mechanism for such macroscopic particles. In Ref. 3, several mechanisms for platelet transport to the surface are considered. It is shown that direct impingement of the platelets as they are carried by the flow to the surface along streamlines is a negligible contribution to the platelet arrival rate and is inadequate to explain observed platelet growth. Similarly, because the platelet is so large compared to molecular species, the diffusion by Brownian motion is very small. The random diffusion coefficient for platelets is roughly 10^{-9} cm^2/sec. compared to $\sim 10^{-5}$ cm^2/sec for low molecular weight species, and hence the flux of particles by ordinary diffusion is very small.

The important transport mechanism is redcell augmented diffusion. The shearing motion of the velocity gradient in the boundary layer causes the red cells, both as individuals and in rouleaux, to tumble at a rate proportional to the velocity gradient. The velocity perturbations caused by

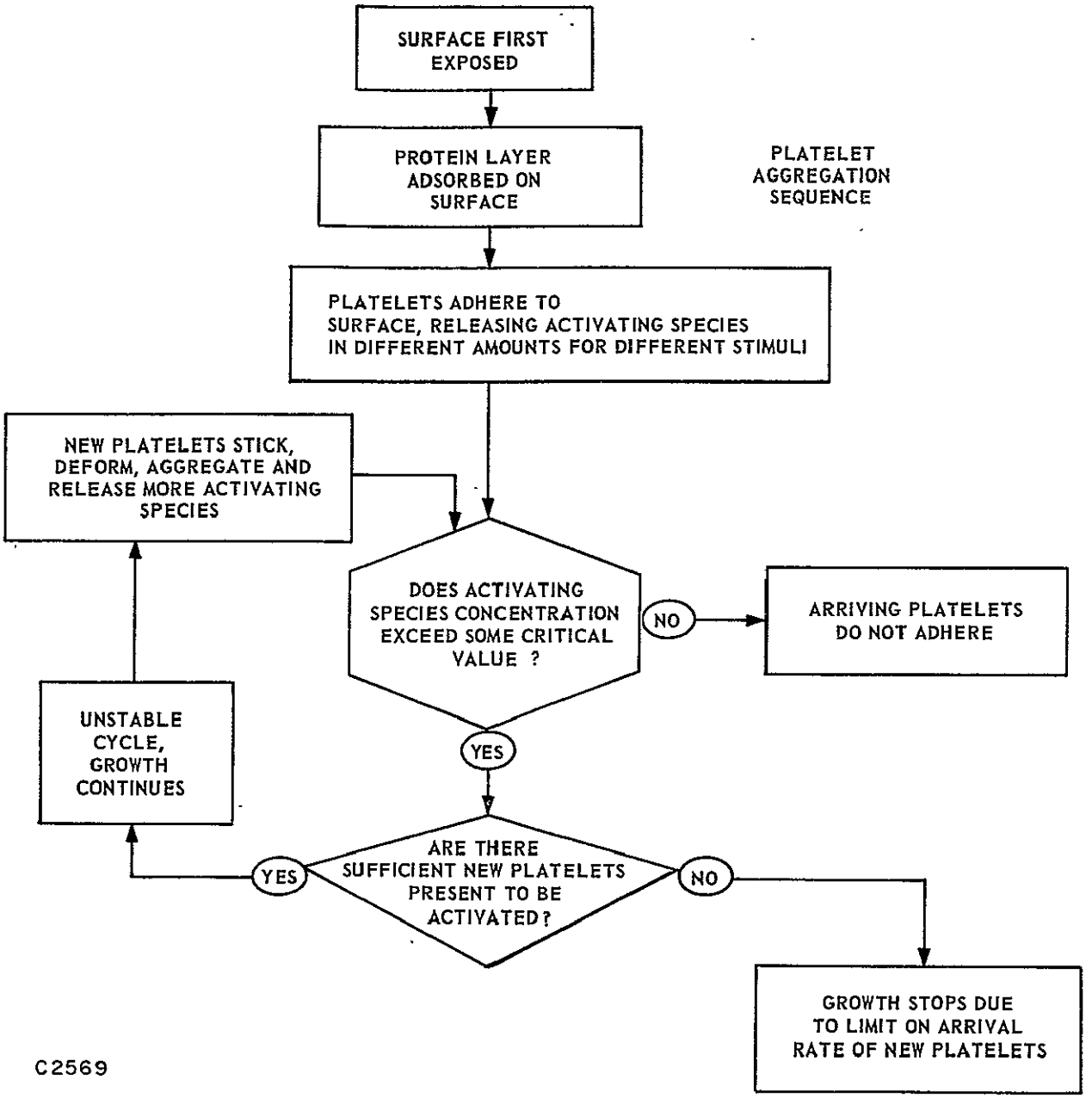

Fig. 22 Platelet aggregation sequence.

these rotating disk-like cells result in a significant enhancement in the mixing rate, not unlike turbulence in nature. The essential effect of the velocity perturbations induced by the red cells rotating in response to the velocity gradient is to make the augmented diffusion coefficient also proportional to the velocity gradient.

The first order effects of red cell tumbling will be estimated with a fairly elementary model. Due to the velocity gradient $(\partial u/\partial z)$ in the boundary layer, a red cell rotates about its diameter with an average angular velocity $\omega = \frac{1}{2}\frac{\partial u}{\partial z}$, as required by a zero net torque on the particle. The velocity field consists of two components; one due to unbounded shear flow, and one due to particle rotation. Representing the rotating red cell as a sphere of radius b, the latter perturbation decreases with distance[13] as $\sim (b/r)^2$, whereas the former varies as $\sim (b/r)^4$. For dilute suspensions (low hematocrit), the only long-range effect is due to red cell rotation, and the effects of red cell interactions are also negligible. Completely random interactions between the small particles (platelets) and the red cell velocity fields will be assumed, with a characteristic frequency f and "mean free time" t given by the relative velocity Δu and average distance $\overline{\Delta r}$ between the red cell and particles:

$$f = \frac{1}{t} = \frac{\Delta u}{\Delta r}$$

hence

$$t = \frac{\overline{\Delta r}}{2\omega\ \overline{\Delta z}} = \frac{1}{2\ \omega}$$

Furthermore, $\overline{\Delta r} \sim 1/2\ C^{1/3}$, where C is the number density of red cells. Finally, the characteristic velocity perturbation is $q' \sim \omega b\ (b/2\overline{\Delta r})^2$. Now, for a "random walk" process, the "mean free path" $\lambda \sim (Dt)^{1/2}$ where D is the diffusivity. Since $\lambda \sim q' t$ as well,

$$D \sim (q')^2 t \sim 8\,\omega^2 b^2 (b/2\,\overline{\Delta r})^4$$

or

$$D \sim 4b^6\ C^{4/3}\ \partial u/\partial z$$

Finally, in terms of the volumetric concentration C_p,

$$D \sim b^2 C_p^{4/3} \partial u/\partial z \tag{18}$$

with the constant of proportionality expected to be of the order one.

The above result is an estimate which is valid, at best, at low hematocrit, for unbounded flows, and small red cell Reynolds number.

In Ref. 21 it is shown that this derived diffusion coefficient is a good approximation to data taken in a simulation experiment using neutrally buoyant spheres in a pipe flow geometry even at moderately high particle concentrations, velocity gradients and particle Reynolds number.

At very low shears this type of diffusion coefficient is inappropriate because the red cells form rouleaux, i. e., they cling together in long chains resembling a stack of poker chips. The diffusion coefficient varies as the square of the largest radius of the particle, so that an increase in particle (rouleaux) length with decreasing shear will reduce the dependence of the diffusion coefficient on the shear.

A model[22] of rouleaux formation that appears to correlate blood viscosity data at low shear yields the following expression for the length to diameter ratio J:

$$J \approx 1 + \frac{5}{4}\left(\frac{\partial \hat{u}}{\partial z}\right)^{-1/2} \tag{19}$$

Thus, as $\partial u/\partial z \to 0$, $J \to (\partial u/\partial z)^{-1/2}$ and the proper length in Eq. (18) is

$$J b \sim \left(\frac{\partial u}{\partial z}\right)^{-1/2}$$

A diffusion coefficient limit at very small shear rates is then obtained:

$$D \to 2 C_p^{4/3} (Jb)^2 \frac{\partial u}{\partial z} \sim 3 C_p^{4/3} b^2$$

For normal blood, then

$$D \to 1.5 \times 10^{-7} \text{ as } \partial u/\partial z \to 0$$

As shear rate increases, $J \rightarrow 1$, and the previous result is obtained. A reasonable matching point is at $\partial u/\partial z = 1.0$, so that

$$D \approx B\,(\partial u/\partial z)^M$$

and

$$B = 1.5 \times 10^{-7}$$

$$M = \begin{cases} 0 \text{ for } \partial u/\partial z \leq 1 \\ 1 \text{ for } \partial u/\partial z \geq 1 \end{cases} \tag{20}$$

The equation expressing the conservation of platelets is the usual steady state boundary layer species conservation equation, which is written as

$$u(r,\ z)\frac{\partial C_p}{\partial r} + v(r,\ z)\ \frac{\partial C_p}{\partial z} = \frac{\partial}{\partial z}\ \left(D\frac{\partial C_p}{\partial z} \right) \tag{21}$$

where C_p is the volumetric concentration of platelets and u, v are the local velocity components in the momentum boundary layer which are given in Sec. IV. Azimuthal and radial diffusion terms have been dropped as being small compared to the normal diffusion, and the term involving an azimuthal velocity will not be present until the thrombus is large enough to appreciably distort the flow. There are no production or loss terms in this equation because the only loss of platelets is at the bounding surface. The outer boundary conditions are that the concentration of platelets assumes the free stream value on the axis and at the edge of the boundary layer

$$C_p\ (r=0,\ z) = C_{p\infty},\ \lim_{z\,\text{large}}\ C_p(r, z) = C_{p\infty} \tag{22}$$

The surface boundary condition we shall leave for later consideration.

In Ref. 2, a similarity solution to Eq. (21) is obtained in order to get the flux of platelets driven to the surface by the augmented diffusion. This flux can be shown to be, for a Newtonian boundary layer and M = 1

$$F_w = D_p \left| \frac{\partial C_p}{dz} \right|_w \frac{\text{platelets}}{\text{cm}^2 \text{sec}} \tag{23}$$

$$= 2 \times 10^{-4} C_{p_\infty} \; (A \sec^{-1})^{5/3} \; (r, \text{ cm})^{2/3}$$

The rate of growth of the thrombus in the z direction can be estimated then to be $\frac{dh}{dt}$ = (flux of platelets to thrombus) (volume of platelet)

$$= F_w \, (4 \times 10^{-12} \text{cm}^3) \tag{24}$$

$$= (8 \times 10^{-16}) \, A^{5/3} \, (r, \text{ cm})^{2/3} \, C_{p_\infty} \text{ cm/sec}$$

For thrombus C, and $A = 17 \sec^{-1}$, $r = 0.155$ c, and $C_{p_\infty} = 4.6 \times 10^8$ cm^3. The rate of increase of height of the thrombus is 5×10^{-6} cm/sec or 3 microns/min. The estimates of observed thickness indicate a smaller rate of growth, like one micron per minute. The halfwidth of thrombus C grew at a rate of about 15 microns/min, however. (See Fig. 18). Since the growth rate calculated should be the maximum rate of accumulation of platelets, it is apparent that the rate of platelet aggregation is probably not limited by platelet arrival rate but rather by the diffusion of activating species.

The equation for the conservation of an activating species has a similar form, only now the diffusion in each of the three directions can be of the same magnitude, so the equation has the form.

$$\frac{\partial C_a}{\partial t} + u(r,z) \frac{\partial C_a}{\partial r} + v(r,z) \frac{\partial C_a}{\partial z} \tag{25}$$

$$= D_a \left\{ \frac{1}{r} \frac{\partial}{\partial r} \left(r \frac{\partial C_a}{\partial r} \right) + \frac{1}{r^2} \frac{\partial^2 C_a}{\partial z^2} \right\}$$

where C_a is the volumetric concentration of activating species and D_a is the corresponding diffusion coefficient, which will be taken to be a constant. We may not, in general, omit the time dependent term here because the concentration contours follow the thrombus surface quite closely and the thrombus growth time history is what we seek. The outer boundary conditions for C_a are that C_a vanishes for large distances from the thrombus in each direction. The initial condition is that C_a vanishes everywhere initially, except at the initiation point of the thrombus ($r = r_i$, $\theta = 0$), at which point it has some given value which is greater than a critical concentration for platelet aggregation.

The phenomenon of the thrombus exuding a particular species which in turn diffuses into and is convected by the boundary layer flow has several interesting features. One can best discuss the various regimes of interest in a coherent manner by reference to the Thrombus Growth Map in Fig. 23. The various shapes of thrombi in a stagnation point flow are illustrated. For early time and for radii of the same size or smaller than a diffusion length, the thrombus is diffusion dominated and will tend to have near equal lateral and radial dimensions. For large flow parameters or for points of initiation large compared to a diffusion length, the thrombus is convection dominated and appears to have a very swept-back shape.

We can get an estimate of the velocity of the thrombus edge growth (the moving platelet aggregation front) in the following way. Assuming that the thrombus is exuding the activating species, at some time τ the locus of the contour of constant critical concentration of this species is assumed to be at a distance δ from the current thrombus position. The thickness of this diffusion layer must depend on a balance between the diffusion perpendicular to the layer and the velocity component perpendicular to the thrombus edge. A good estimate of the size of this diffusion layer is

$$\delta \approx \frac{D_a}{u(r, z) \cos \alpha} \tag{26}$$

where α is the angle between the direction of the boundary layer velocity vector and the thrombus edge normal. There is a question as to what vecocity to use here, i. e., how far up into the velocity boundary layer does

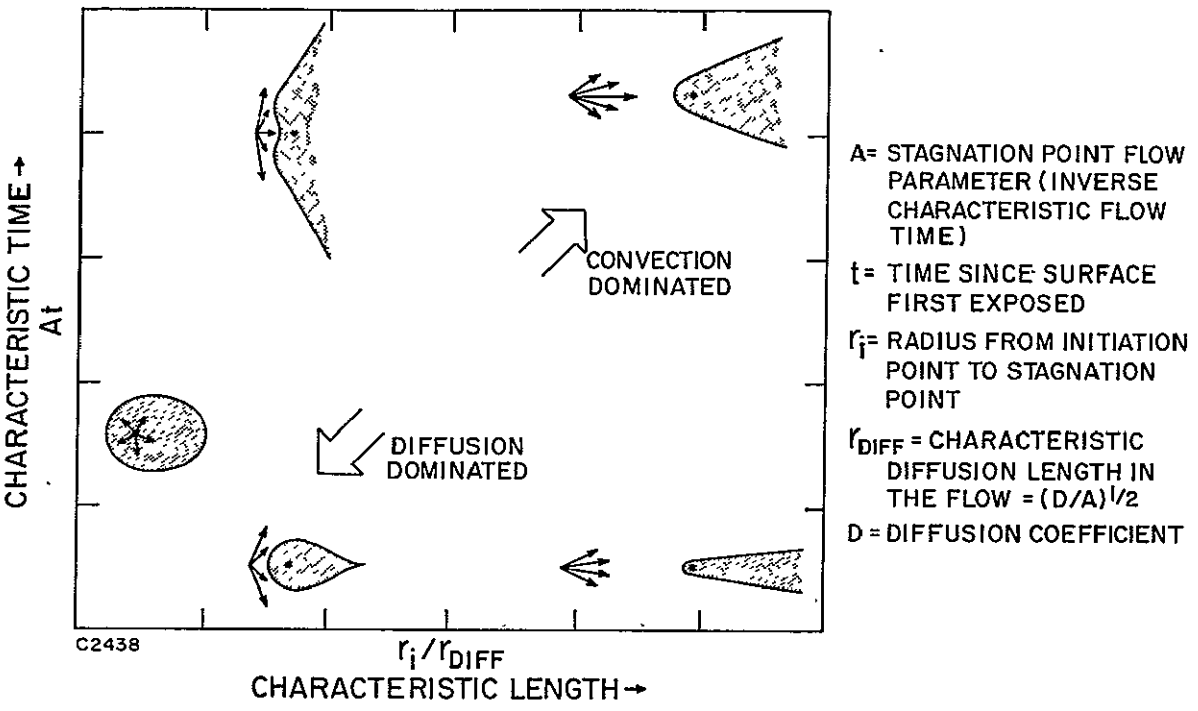

Fig. 23 Wedge thrombus growth map.

this diffusion process extend? It must be of the same order as the sideways diffusion, so we evaluate the velocity in the boundary layer at a height equal to δ. We shall use

$$u(z = \delta) = \frac{\partial u}{\partial z}\ \delta = \frac{Ar\ \phi''(0)\ \delta}{\sqrt{\nu / A}} \qquad (27)$$

for the velocity in the boundary layer in the previous formula for diffusion thickness. Solving for δ then gives

$$\delta = \left(\frac{D_a}{\frac{\partial u}{\partial z} \cos \alpha} \right) = \left(\frac{D_a\ \nu^{1/2}}{A^{3/2}\ \phi''(0) r \cos \alpha} \right)^{1/2} \qquad (28)$$

This is a measure of the distance in which the diffusion front moves in the time $\left(\frac{\partial u}{\partial z} \cos \alpha \right)^{-1}$ and defines the region within which the concentration of activating species is above some critical level. This region will march forward in time as platelets arrive within the region, stick, and release more of the species. We can estimate the characteristic time τ for the surface to collect a particular surface density of platelets by making the ratio of the flux to the wall of platelets to the surface density of platelets. This surface density should properly be that necessary to release the critical concentration of the activating species. This would be a very interesting number to derive from the measured growth velocity data once this simple model is complete.

Then

$$\frac{1}{\tau} \approx \frac{F_w}{N_{pw}} = \frac{D_p}{N_{pw}} \frac{\partial C_p}{\partial z} \quad \sec^{-1} \qquad (29)$$

is a fair estimate of the characteristic time to deposit a particular surface density of platelets.

The velocity of the edge of the thrombus is the distance in which the region δ of sufficient activating species advances as it fills up with platelets in time τ. This speed is

$$u_{th} = \frac{\delta}{\tau} = \frac{D_p}{N_{pw}} \frac{\partial C_p}{\partial z} \left(\frac{D_a}{\frac{\partial u}{\partial z} \cos \alpha} \right)^{1/2} \tag{30}$$

In the Newtonian region where the platelet diffusion is augmented M = 1 and the flux is

$$F_w = D_p \frac{\partial C_p}{\partial z} = \frac{A^{3/2}}{4\sqrt{\nu}} (Br)^{2/3} C_{p_\infty} \tag{31}$$

So the thrombus front velocity is

$$u_{th} = \frac{A^{3/4}}{4} \frac{C_{p_\infty}}{N_{pw}} (B^2 r^{1/2})^{1/3} \left(\frac{D_a}{\nu^{1/2} \phi''(0) \cos \alpha} \right)^{1/2} \tag{32}$$

The dependence of the growth velocity on the parameters is very interesting. The strongest dependence is on the flow parameter and on the platelet free stream concentration with lesser dependence on the species diffusivities and radius.

The required surface density of platelets to get a critical concentration of activating species is taken as $N_{pw} = 1.5 \times 10^5$ platelets/cm^2. Friedman[7], for example, quotes about 70×10^5 platelets/cm^2 total surface density deposited after six minutes or so. These numbers are consistent in the sense that the number of platelets necessary per unit area to continue the growth of the aggregation region is likely to be smaller than the total surface density already there.

Note that the geometrical factors in the growth velocity, $u_{th} \sim r^{1/6} \cos^{-1/2} \alpha$, would indicate fastest growth where the edge is aligned with the flow (large α) and at larger radii, which is consistent with our observations.

The expression for the thrombus growth velocity in (32) should collapse the data taken for the four thrombi at different flow conditions. Taking $u_{th} = dr/dt$ and integrating to find the front position versus time, $r(t)$, we get

$$\frac{(r^{5/6} - r_i^{5/6}) \cos^{1/2} \alpha}{A^{3/4} t} = \frac{5}{24} \frac{C_{p_\infty} B^{2/3}}{N_{pw}} \left(\frac{Da}{\nu^{1/2} \phi''(0)} \right)^{1/2} \quad (33)$$

The factors on the right hand side of the equation are fixed constants for any blood sample. The factors on the left side are the scaling factors for thrombus position as a function of time and angular position for different flow parameters.

In Fig. 20 we have graphed the thrombus head position as a function of time for the four thrombi grown under different flow conditions. The agreement is excellent considering the uncertainties in the concentrations and diffusivities.

Part II: Late Time

The asymptotic structure of a growing wedge thrombus is characterized by a large number of well define platelet aggregates. As seen in Figs. 9, 10 and 11, the aggregates form in the wake of the initial disturbance (thrombus head) and grow with time. As they grow, their total number decreases, and the interaggregate distance increases. Thus, the ratio of aggregate size to separation distance appears to be fairly constant with time, and the characteristics aggregate dimensions apparently "scale" with thrombus size. Since aggregate growth has been shown[3] to be due primarily to platelet diffusion induced by red cell tumbling, it is possible that this mechanism is also responsible for the observed aggregate geometry. An aggregate's growth is enhanced at its peak and reduced in the valleys between aggregates[3], due to the dependence of platelet "diffusivity" on the local velocity gradient. Thus, the aggregates steepen as they grow, until the velocity gradient and diffusivity vanish in the valleys at a critical value of the ratio of aggregate size to separation distance. For longer times, an aggregate surface area with positive platelet flux is constantly reduced, and its ultimate size is soon attained. For a given aggregate half-wavelength λ,

there is a characteristic time when the aggregate "sharpens" and achieves its maximum height. To estimate this time, consider the approximate solution[3] for the velocity gradient distribution on the wavy wall representing an array of aggregates shown in Fig. 24.

$$\left(\frac{\partial u}{\partial z}\right)_w \simeq \left(\frac{\partial u}{\partial z}\right)_\infty \left[1 + \frac{2\pi\epsilon}{\lambda} \sin\frac{\pi r}{\lambda}\right] \tag{34}$$

When $\frac{\epsilon}{\lambda} \simeq 1/2\pi$, the velocity gradient vanishes in the valleys and is enhanced by a factor of two at the peaks. As the aggregate grows, the growth rate increases at the peaks, since the diffusivity is given by

$$D_w = B\left(\frac{\partial u}{\partial z}\right)_w \text{ cm}^2/\text{sec}$$

and the platelet concentration gradient, for constant particle flux between streamlines, is given by

$$\begin{aligned}\left(\frac{\partial c}{\partial z}\right)_w &\simeq \left(\frac{\partial c}{\partial z}\right)_\infty \sqrt{\left(\frac{\partial u}{\partial z}\right)_w / \left(\frac{\partial u}{\partial z}\right)_\infty} \\ &\simeq \left(\frac{\partial c}{\partial z}\right)_\infty \left[1 + \frac{\pi\epsilon}{\lambda} \sin\frac{\pi r}{\lambda}\right]\end{aligned} \tag{35}$$

Therefore, a first-order approximation of the platelet flux to the wall is

$$\begin{aligned}F_w &= D_w \left(\frac{\partial c}{\partial z}\right)_w \\ &\approx B\left(\frac{\partial u}{\partial z}\right)_\infty \left(\frac{\partial c}{\partial z}\right)_\infty \left[1 + \frac{3\pi\epsilon}{\lambda} \sin\frac{\pi r}{\lambda}\right]\end{aligned} \tag{36}$$

The aggregate growth rate is then approximated by:

$$\frac{\partial z_w}{\partial t} \approx V_p B \left(\frac{\partial u}{\partial z}\right)_\infty \left(\frac{\partial c}{\partial z}\right)_\infty \left[1 + \frac{3\pi\epsilon}{\lambda} \sin\frac{\pi r}{\lambda}\right] \tag{37}$$

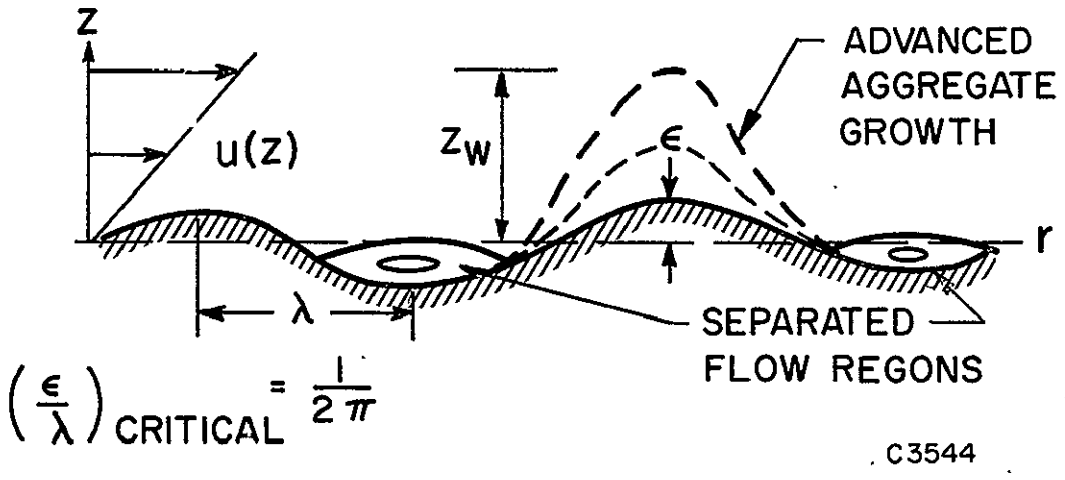

Fig. 24 Schematic of platelet aggregate array growth model.

where V_p is the volume of a platelet, $\sim 4 \times 10^{-12}$ cm^3. Since the above equation is valid to first-order for $t > 0$, the following solution is found:

$$z_w = \lambda \bar{t} + \epsilon_o \exp\left[3\pi\bar{t}\right] \sin \frac{\pi r}{\lambda} \tag{38}$$

where $$\lambda \bar{t} = V_p B \left(\frac{\partial u}{\partial z}\right)_\infty \left(\frac{\partial c}{\partial z}\right)_\infty t$$

with ϵ_o the amplitude at $t = o$.

The first term in the equation above represents uniform growth of the aggregates, while the second term describes the unstable growth of the peaks. It is the second term that limits the growth of an aggregate, and this occurs on the time scale given by

$$\bar{t} \sim 1/3\pi$$

The characteristic growth time is therefore

$$\tau_G = \lambda \left[3\pi B V_p \left(\frac{\partial u}{\partial z}\right)_\infty \left(\frac{\partial c}{\partial z}\right)_\infty\right]^{-1}$$

Thus, the time to grow a mature aggregate of wavelength 2λ is τ_G. Conversely, the maximum aggregate growth in a time τ_G is to be expected for aggregates separated by a distance of 2λ, defined above. Denoting this distance as $2\lambda_G$, it follows that for $\lambda < \lambda_G$ growth stops at $t < \tau_G$, while for $\lambda > \lambda_G$ the growth rate is less than that for λ_G. Thus, with increasing time, the initial large number of small closely spaced aggregates should be replaced by fewer large aggregates, with greater separation.

While the above conclusion is in qualitative agreement with experimental observations, it remains to be shown that the calculated platelet flux, when used in Eq. (39), is consistent with the growth of aggregate height and interaggregate distance with time. For a sufficiently larger shear rate, e.g., outside the white cell circle, the Newtonian flow field solution[3] may be used. The unperturbed platelet flux then becomes:

$$B \left(\frac{\partial u}{\partial z}\right)_{\infty} \left(\frac{\partial c}{\partial z}\right)_{\infty}$$

$$= (1.5 \times 10^{-7} r)^{2/3} c_{\infty} A^{3/2} \tag{40}$$

Taking $c_{\infty} = 4.6 \times 10^{8}$ platelets/cm^3, the flux at $A = 9$ sec^{-1}, $r_i = 0.9$ mm is 8×10^{4} platelets/cm^2 - sec and the expected interaggregate distance is

$$2\lambda_G \approx .05 \tau_G (\text{microns}) \tag{41}$$

To compare this calculation with experimental data, the distribution of interaggregate distances (taking all adjacent aggregate pairs) was measured at three times in a thrombus formed at the above conditions. This data is presented in Fig. 21, with a "best fit" curve drawn through each set. The interval of 2λ with the maximum number of aggregates is taken as the characteristic interaggregate distance, and is compared with $2\lambda_G$ in Fig. 25. The data are seen to be in remarkable agreement with the theoretical result, particularly in view of the many approximations involved in the analysis. It should also be noted that there appears to be, as expected, a slight dependence of 2λ on radial and angular location in the thrombus. The latter effect is demonstrated by the double-peaked distribution in Fig. 21 which reflects the "age" of aggregates along the azimuthally growing edges of the thrombus.

Two additional observations strengthen the model of aggregate growth described. First, the other possible growth mechanism, that of direct interception of platelets by aggregates, yields a growth rate that is an order-of-magnitude smaller than the diffusion rate. Second, the ability of platelet aggregates to trap red cells in their valleys depends on development of low velocity, low shear regions that are approximately an order-of-magnitude larger than the red cell diameter (8μ). Since red cell trapping (and reverse flow in some cases) is observed, and at times when both calculated and measured to be in the $\sim 50\mu$ range, there is little doubt that the aggregate and its surrounding flow field behave in the manner described.

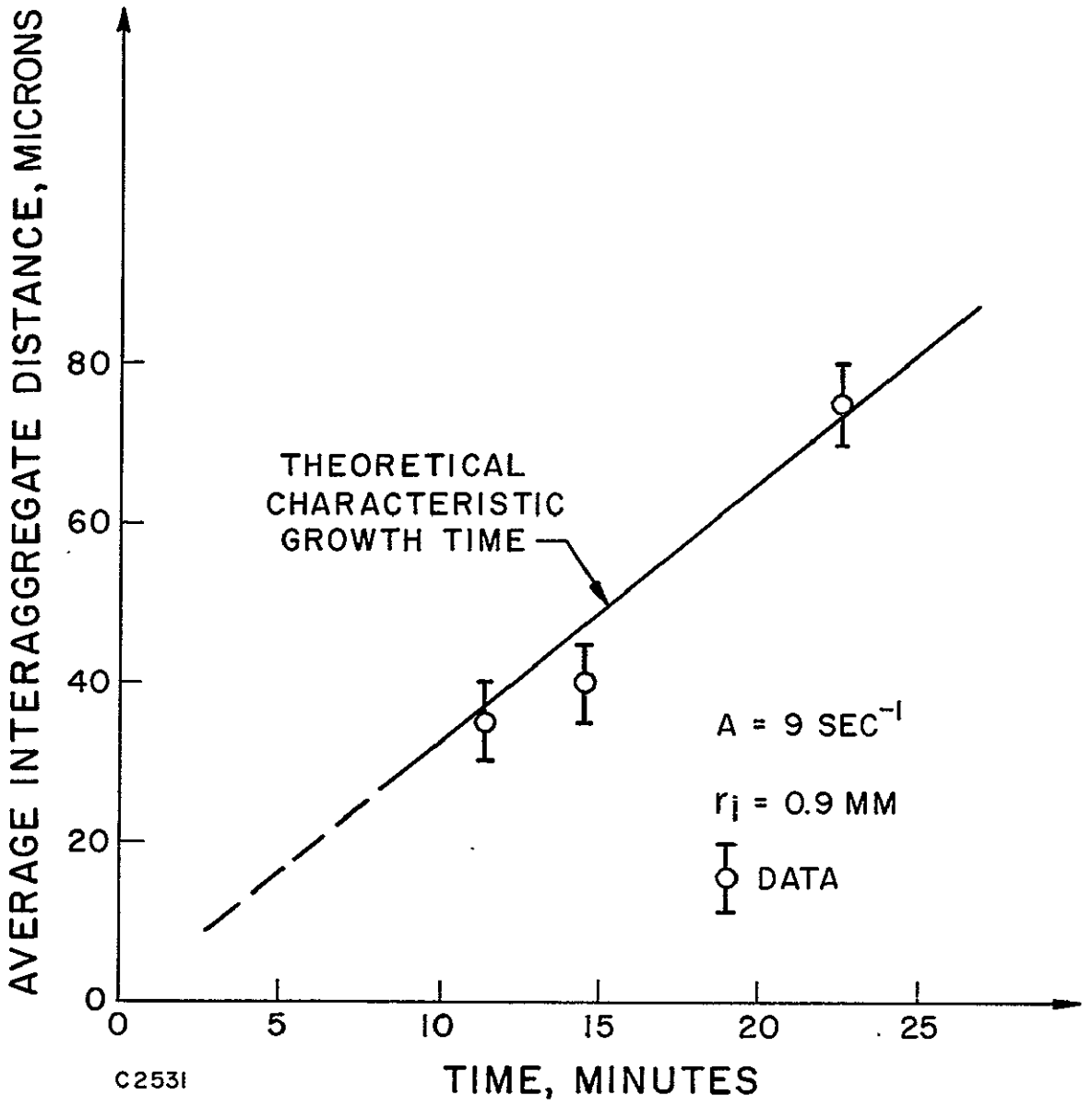

Fig. 25 Interaggregate distance as a function of time.

In summary, it appears that platelet aggregates grow by an unstable diffusion/surface shape interaction, interaggregate distances scale with the local platelet flux rate and time, and the growth pattern is responsible for red cell trapping. Further investigations should consider the effects of three-dimensional aggregate arrays, more general growth patterns, and specific platelet aggregation mechanisms.

VII. CONCLUDING DISCUSSION

The experimental data we have shown for the shape, size and growth rate of a thrombus on a foreign surface clearly show the effects of the flow of the blood on thrombus growth. Our understanding of the physical processes affecting the evolution of a thrombus, though hindered by the lack of knowledge of the detailed chemistry, has been increased by the application of simple fluid mechanical and mass transfer models. The basic concept underlying the growth model is the existence of a balance between the rate at which an activating species diffuses and is convected from the thrombus and the rate at which new platelets can diffuse from the flowing blood to the surface. The flow dependence of this platelet diffusion rate is emphasized as the growth rate limiting factor, and the diffusion and convection of an activating species is shown to control the shape.

The asymptotic character of the thrombus growth is treated and succeeds in demonstrating the flow dependence of the size and spacing of aggregates, as well as their role in trapping the larger red cells. Though the effect of the type of surface material is not considered, we note the role of a surface inhomogeneity in triggering the initial platelet aggregation leading to the thrombus. The platelet aggregation is shown to have an unstable "switch-on" nature which occurs when the critical concentration of activating species is exceeded. It seems that a smooth artificial surface sufficiently free of surface imperfections may be quite non-thrombogenic under some flow conditions even if it does not prevent clot formation of stagnant blood. To settle questions of this type, further experimentation and mathematical modeling is certainly needed.

Acknowledgment

The authors gratefully acknowledge the contributions and suggestions of P. Madras and the assistance of R. DeRocher, Jr. in the laboratory.

REFERENCES

1. Monsler, M., Morton, W., and Weiss, R., "The Fluid Mechanics of Thrombus Formation" presented at the 3rd AIAA Fluid and Plasma Dynamics Conference, Los Angeles, Calif., June 1970, AIAA Paper No. 70-787.

2. Madras, P.N., Morton, W., and Petschek, H., "The Dynamics of Thrombus Formation" presented at the Conference on Boundary Effects on Moving Blood," San Diego, Calif., 13-15 January 1971, to be published in Federation Proceedings. Also Avco Everett Research Laboratory Research Report 365.

3. Petschek, H.E. and Weiss, R.F., "Hydrodynamic Problems in Blood Coagulation," presented at the AIAA 8th Aerospace Sciences Meeting, New York, New York, January 1970, AIAA Paper No. 70-143.

4. Petschek, H.E., Adamis, D. and Kantrowitz, A., "An Experimental Preparation for the Study of Thrombus on Artificial Surfaces under Controlled Flow Conditions," Avco Everett Research Laboratory Research Report 314 (September 1968).

5. Petschek, H., Adamis, D., and Kantrowitz, A.R., "Stagnation Flow Thrombus Formation," Trans. Amer. Soc. Artif. Int. Organs, Vol. 14, pp. 256-260 (1968).

6. Petschek, H.E. and Madras, P.N., "Thrombus Formation on Artificial Surfaces," in Proceedings of the National Heart Institute Artificial Heart Program Conference (June 1969).

7. Friedman, L.I., Liem, H., Grabowski, E.F., Leonard, E.F., and McCord, C.W., "Inconsequentiality of Surface Properties for Initial Platelet Adhesion," to be published in Trans. Amer. Soc. Artif. Int. Organs, 1970.

8. French, J.E., "The Fine Structure of Experimental Thrombi," Thrombosis, ed. by S. Sherry, K.M. Brinkhous, E. Genton, and J.M. Stengle, pp. 300-321, National Academy of Sciences, Washington, D.C. (1969).

9. Obrien, J.R., "The Properties of the Platelet Membrane," Dynamics of Thrombus Formation and Dissolution, ed. by S.A. Johnson, and M.M. Guest, pp. 121-148, Lippincott, Philadelphia (1969).

10. Sherry S., Brinkhous, K.M., Genton, E., Stengle, J.M., ed. Thrombosis, National Academy of Sciences, Washington, D.C. (1969).

11. Zucker, M.B., "Platelet Aggregation and Release Reactions Induced by Adenosine Diphosphate and Other Physiologic Substances," Thrombosis, ed. by Sherry, S., Brinkhous, K.M., Genton, E., and Stengle, J.M., pp. 300-321, National Academy of Sciences, Washington, D.C. (1969).

12. Johnson, S.A. and Guest, M.M., ed. Dynamics of Thrombus Formation and Dissolution, Lippincott, Philadelphia (1969).

13. Marcus, A.J. and Zucker, M.B., The Physiology of Blood Platelets, Grune & Stratten Inc., New York (1965).

14. Kowalski, E. and Niewiarowski, S., ed. Biochemistry of Blood Platelets, Academic Press, New York (1967).

15. Johnson S.A., Monts, R.W., Rebuck, J.W., and Horn, R.C., Jr., Blood Platelets, Henry Ford Hospital International Symposium, Little, Brown & Company, Boston, Massachusetts (1961).

16. Schlichting, H., Boundary Layer Theory, 4th ed., pp. 81-83, McGraw-Hill, New York (1960).

17. Merrill, E.W., Margetts, W.G., Cokelet, G.R., and Gilliland, E.R., "The Casson Equation and Rheology of Blood Near Zero Shear," Symposium on Biorheology, Proceedings of 4th International Congress on Rheology, ed. by A. Copley, pp. 135-143, Interscience, New York City (1965).

18. Rahn, A.W., Tien, C. and Cerny, L.C., "Flow Properties of Blood Under Low Shear Rate," Chemical Engineering in Medicine and Biology, ed. by D. Hershey, pp. 45-83, Plenum Press, New York City (1967).

19. Bugliarello, G., Kapur, C. and Hsias, G., "The Profile Viscosity and Other Characteristics of Blood Flow in a Non-uniform Shear Field," Symposium on Biorheology, Proceedings of 4th International Congress on Rheology, ed. by A. Copley, pp. 351-370, Interscience, New York City (1965).

20. Kim, K.H. and Erasian, A.H., "Non-Newtonian Stagnation Flow with Mass Injection," Journal of Hydronautics, Vol. 2, No. 4 (October 1968)

21. Collingham, R.E., "Mass Transfer in Flowing Suspensions," Ph.D. Thesis, University of Minnesota, University Microfilms, Inc. (1968).

22. Merrill, E. W., Margetts, W. G., Cokelet, G. R., and Gilliland, E. R., "The Casson Equation and Rheology of Blood Near Zero Shear," Symposium on Biorheology, Proceedings of 4th International Congress on Rheology, ed. by A. Copley, pp. 135-143, Interscience, New York City (1965).

23. Vand, V., J. Phys. Colloid Chem., Vol. 52, p. 277 (1948), in Ref. 4, p. 150; also, see Rubinow, S. I. and Keller, J. B., The Transverse Force on a Spinning Sphere Moving In a Viscous Fluid," Journal of Fluid Mechanics, Vol. 11, Part 3, p. 447-459 (1961).